

CRFIEKF: An Efficient Parameter Estimation Method for Biochemical Pathway Modeling

Abhisek Bakshi¹, Abhijit Dasgupta^{2*}, Souvik Sengupta^{3*}, and Rajat K. De^{4*}

¹Department of Research and Development, Michelin India Private Limited, World Trade Center, Tower 4, Kharadi, MIDC Knowledge Park, Pune 411014, India;

²Department of Structural Biology, St. Jude Children's Research Hospital, 262 Danny Thomas Place, MS 311, Memphis, TN 38105, USA;

³Department of Computer Science and Engineering, Aliah University, Kolkata 700156, West Bengal, India;

⁴Machine Intelligence Unit, Indian Statistical Institute, 203 B.T. Road, Kolkata 700108, India.

Supplementary Material

1. Algorithm

Algorithm 1.1: CRFIEKF algorithm (l_1 regularization): Assuming there are ‘m’ number of state components in the extended biochemical pathway. Besides, we consider ‘n’ number of approximated measurements are available to us.

```
Data:  $\hat{x}_0^{' +}, \widehat{W}_0^+, \mathcal{R}_\epsilon, N_\tau$ 
Result: k
1  $D \leftarrow -I$ 
2  $\vec{d} \leftarrow 1$ 
3  $iter \leftarrow 0$ 
4  $time \leftarrow [0 : 0.002 : 10]$ 
5 while  $p \leq limit$  do
6    $\mathcal{J}_p^f \leftarrow Jacobean(time(p), \hat{x}_p^{' +})$ 
7    $\dot{\hat{x}} \leftarrow f(\hat{x}', \mathbf{u}) \quad \text{where } \hat{x}'(t_{p-1}) \leftarrow \hat{x}_{p-1}^{' +}$ 
8    $\hat{x}_p^{' -} \leftarrow \hat{x}'(t_p)$ 
9    $\widehat{W} \leftarrow P(\mathcal{J}_p^f, \mathbf{W}, \mathcal{Q}) \quad \text{where } \mathbf{W}(t_{p-1}) \leftarrow \widehat{W}_{p-1}^+$ 
10   $\widehat{W}_p^- \leftarrow \mathbf{W}(t_{p-1})$ 
11   $\mathcal{G}_p \leftarrow \widehat{W}_p^- \mathcal{J}_p^{hT} (\mathcal{J}_p^h \widehat{W}_p^- \mathcal{J}_p^{hT} + \mathcal{R})^{-1}$ 
12   $\mathbf{z}_p \leftarrow FIS(\hat{x}_p^{' -})$ 
13   $\hat{x}_p^{' +} \leftarrow \hat{x}_p^{' -} + \mathcal{G}_p(\mathbf{z}_p - h(\hat{x}_p^{' -}))$ 
14   $\widehat{W}_p^+ \leftarrow (I - \mathcal{G}_p \mathcal{J}_p^h) \widehat{W}_p^- (I - \mathcal{G}_p \mathcal{J}_p^h)^T + \mathcal{G}_p \mathcal{R} \mathcal{G}_p^T$ 
15   $\widehat{W}_{reg} \leftarrow \widehat{W}_p^+$ 
16   $\hat{x}_{reg}^{' +} \leftarrow \hat{x}_p^{' +}$ 
17  while  $\tau \leq N_\tau$  do
18     $\bar{\mathcal{H}} \leftarrow [\xi(1\hat{x}_p^{' +}), \xi(2\hat{x}_p^{' +}), \dots, \xi((m+n)\hat{x}_p^{' +})]$ 
19     $\mathcal{K}_{RFIEKF} \leftarrow \widehat{W}_{reg} \bar{\mathcal{H}}^T (\bar{\mathcal{H}} \widehat{W}_{RFIEKF} \bar{\mathcal{H}}^T + \mathcal{R}_\epsilon)^{-1}$ 
20     $\hat{x}_{RFIEKF}^{' +} \leftarrow (I - \mathcal{K}_{reg} \bar{\mathcal{H}}) \hat{x}_{RFIEKF}^{' +}$ 
21     $\widehat{W}_{RFIEKF} \leftarrow (I - \mathcal{K}_{RFIEKF} \bar{\mathcal{H}}) \widehat{W}_{RFIEKF}$ 
22  end
23   $\widehat{W}_p^+ \leftarrow \widehat{W}_{reg}$ 
24   $\hat{x}_p^{' +} \leftarrow \hat{x}_{reg}^{' +}$ 
25  if  $D\hat{x}_p^{' +} \leq d$  then
26     $c\hat{x}_p^{' +} \leftarrow \vec{d} - D\hat{x}_p^{' +}$ 
27     $cons \leftarrow Quadratic\_programming(\widehat{W}_p^+, D, c\hat{x}_p^{' +})$ 
28     $\hat{x}_p^{' +} \leftarrow \hat{x}_p^{' +} + cons$ 
29  else
30    | Continue
31  end
32 end
```

* Correspondence should be addressed to Rajat K. De, Ph.D., Machine Intelligence Unit, Indian Statistical Institute, 203 B.T. Road, Kolkata, West Bengal 700108, India, Email: rajat@isical.ac.in or Souvik Sengupta, Ph.D, Department of Computer Science and Engineering, Aliah University, Kolkata, West Bengal 700156, Email: ssg@aliah.ac.in or Abhijit Dasgupta, Ph.D., Department of Structural Biology, St. Jude Children's Research Hospital, Memphis, TN 38105, USA, Email: Abhijit.Dasgupta@stjude.org.

Algorithm 1.2: CRFIEKF algorithm (Tikhonov regularization): Assuming there are ‘m’ number of state components in the extended biochemical pathway. Besides, we consider ‘n’ number of approximated measurements are available to us.

Data: $\hat{\mathbf{x}}_0^{' +}, \widehat{\mathbf{W}}_0^+, \mathcal{R}, \lambda$
Result: \mathbf{k}

- 1 $D \leftarrow -I$
- 2 $\vec{d} \leftarrow 1$
- 3 $iter \leftarrow 0$
- 4 $time \leftarrow [0 : 0.002 : 10]$
- 5 **while** $p \leq limit$ **do**
- 6 $\mathcal{J}_p^f \leftarrow Jacobean(time(p), \hat{\mathbf{x}}_p^{' +})$
- 7 $\dot{\hat{\mathbf{x}}} \leftarrow f(\hat{\mathbf{x}}^{'}, \mathbf{u}) \quad where \quad \hat{\mathbf{x}}'(t_{p-1}) \leftarrow \hat{\mathbf{x}}_{p-1}^{' +}$
- 8 $\dot{\hat{\mathbf{x}}}_p^{' -} \leftarrow \dot{\hat{\mathbf{x}}}(\mathbf{t}_p)$
- 9 $\widehat{\mathbf{W}} \leftarrow P(\mathcal{J}_p^f, \mathbf{W}, \mathcal{Q}) \quad where \quad \mathbf{W}(t_{p-1}) \leftarrow \widehat{\mathbf{W}}_{p-1}^+$
- 10 $\widehat{\mathbf{W}}_p^- \leftarrow \mathbf{W}(\mathbf{t}_{p-1})$
- 11 $\mathcal{G}_p \leftarrow \widehat{\mathbf{W}}_p^- \mathcal{J}_p^{hT} (\mathcal{J}_p^h \widehat{\mathbf{W}}_p^- \mathcal{J}_p^h + \mathcal{R})^{-1}$
- 12 $\mathbf{z}_p \leftarrow FIS(\hat{\mathbf{x}}_p^{' -})$
- 13 $\hat{\mathbf{x}}_p^{' +} \leftarrow \hat{\mathbf{x}}_p^{' -} + \mathcal{G}_p(\mathbf{z}_p - h(\hat{\mathbf{x}}_p^{' -}))$
- 14 $\widehat{\mathbf{W}}_p^+ \leftarrow (I - \mathcal{G}_p \mathcal{J}_p^h) \widehat{\mathbf{W}}_p^- (I - \mathcal{G}_p \mathcal{J}_p^h)^T + \mathcal{G}_p \mathcal{R} \mathcal{G}_p^T$
- 15 $normal_matrix \leftarrow \mathcal{J}_p^{hT} \mathcal{R}^{-1} \mathcal{J}_p^h + \widehat{\mathbf{W}}_p^+$
- 16 $cond \leftarrow Norm(normal_matrix) * Norm(inv(normal_matrix))$
- 17 **if** $cond \geq Threshold$ **then**
- 18 $\mathcal{G}_p^{RFIEKF} = \mathcal{J}_p^{hT} \mathcal{R}^{-1} \mathcal{J}_p^h + \widehat{\mathbf{W}}_p^+ + \lambda \cdot \widehat{\mathbf{W}}_p^{+ -1}$
- 19 $\hat{\mathbf{x}}_p^{RFIEKF} = \hat{\mathbf{x}}_p^{' -} + \mathcal{G}_p^{RFIEKF}(\mathbf{z}_p - h(\hat{\mathbf{x}}_p^{' -}))$
- 20 $\widehat{\mathbf{W}}_p^{RFIEKF} = (I - \mathcal{G}_p^{RFIEKF} \mathcal{J}_p^h) \widehat{\mathbf{W}}_p^+$
- 21 $\hat{\mathbf{x}}_p^{' +} \leftarrow \hat{\mathbf{x}}_p^{RFIEKF}$
- 22 $\widehat{\mathbf{W}}_p^+ \leftarrow \widehat{\mathbf{W}}_p^{RFIEKF}$
- 23 **else**
- 24 | Continue
- 25 **end**
- 26 **if** $D \hat{\mathbf{x}}_p^{' +} \leq d$ **then**
- 27 $c \hat{\mathbf{x}}_p^{' +} \leftarrow \vec{d} - D \hat{\mathbf{x}}_p^{' +}$
- 28 $cons \leftarrow Quadratic_programming(\widehat{\mathbf{W}}_p^+, D, c \hat{\mathbf{x}}_p^{' +})$
- 29 $\hat{\mathbf{x}}_p^{' +} \leftarrow \hat{\mathbf{x}}_p^{' +} + cons$
- 30 **else**
- 31 | Continue
- 32 **end**
- 33 **end**

Table S1. Different mathematical symbols and their description

$\mathbf{x}, \mathbf{y}, \mathbf{u}$ and \mathbf{k}	Vectors representing input molecule expression/concentration levels, output molecule expression/concentration levels, concentration of external inputs and kinetic parameters respectively.
n'' and q	Number of molecules involved in the known approximate relationship in the biochemical pathway and number of discrete time instant respectively.
p	Index for the discrete time instant.
\mathbf{z}_p	Vectors representing measurement signal, evaluated using known approximated relationship among molecules involved in the biochemical pathway.
n, n', s and m and l	Dimension of $\mathbf{x}, \mathbf{y}, \mathbf{u}, \mathbf{k}$ and \mathbf{z}_p respectively.
i, j and l'	Index for \mathbf{x}, \mathbf{k} and \mathbf{z}_p involved in the biochemical pathway respectively.
\mathbf{x}'	State vector representing expression/concentration levels extended state space model of the biochemical pathway.
\mathbf{x}'_p	State vector representing expression/concentration levels extended state space model of the biochemical pathway at p^{th} time instant.
$\dot{\mathbf{x}}', \dot{\mathbf{k}}$	Derivatives of \mathbf{x}', \mathbf{k} respectively, with respect to time t .
w and v_p	Process noise and measurement noise at p^{th} time instant respectively .
\mathcal{Q} and \mathcal{R}	covariance matrix of w and v_p respectively .
$f(\cdot), h(\cdot)$ and $g(\cdot)$	Nonlinear functions corresponding to input, output and approximate relationship among certain molecules of the extended state space model of the biochemical pathway respectively.
j'	Index of the molecules involved in known approximate relationship among certain molecules of \mathbf{x}'_p .
$c_{j'}' \text{ and } f_{j'}'$	Crisp and fuzzy value of the j'^{th} molecule $x_{j'}' \in \mathbf{x}'_p$ respectively.
$f\mathbf{x}'_p$	The fuzzy set corresponding to \mathbf{x}'_p .
$\underline{x}_{j'}, \mathcal{L}\underline{x}_{j'}, \mathcal{U}\underline{x}_{j'} \text{ and } \mu_{\underline{x}_{j'}}$	linguistic variable of $x_{j'}'$, set of linguistic values that $x_{j'}'$ can take, Universe of discourse of $\underline{x}_{j'}$ and Gaussian membership function for $\underline{x}_{j'}$ respectively.
ε and ρ	Center and width of the fuzzy set $f\mathbf{x}'_p$.
\mathcal{F}_r and r	Number of fuzzy rules and the index of fuzzy rules.
z_p^l	l^{th} measurement signal at p^{th} time instant.
$r z_p^{l'}$	Fuzzy value of $z_p^{l'}$ on applying r^{th} fuzzy rule.
j''	Index of the linguistic values $\in \mathcal{L}\underline{x}_{j'}$ for the fuzzy variable $f_{j'}'$.
$\alpha_{l'}^r$	Firing strength of $r z_p^{l'}$ based on r^{th} fuzzy rule.
\mathbf{W}	Error covariance matrix of CRFIEKF.
$\hat{\mathbf{x}}'^+$ and $\hat{\mathbf{x}}'^-$	a posteriori and a priori estimate respectively of $\hat{\mathbf{x}}$.
$\widehat{\mathbf{W}}^+$ and $\widehat{\mathbf{W}}^-$	a posteriori and a priori estimate respectively of error covariance matrix \mathbf{W} .
$\dot{\mathbf{x}}'$ and $\dot{\mathbf{W}}$	Time derivative of x' and \mathbf{W} respectively.
\mathcal{J}_p^f and \mathcal{J}_p^h	Jacobeans of $f(\cdot)$ and $h(\cdot)$ respectively.
\mathcal{G}_p and I	Kalman gain at p^{th} time instant and Identity matrix respectively.
λ, ϵ and \mathcal{R}_ϵ	regularization parameter, kinetic parameter measurement noise and covariance matrix of ϵ respectively.
N_τ	Number of iteration in $l1$ regularization algorithm.
\mathbf{N}_p	Normal matrix of Standard EKF equation.
$C(\mathbf{N}_p)$	Condition number of Normal matrix \mathbf{N}_p .
$\mathcal{G}_p^{CRFIEKF}, \hat{\mathbf{x}}_p^{RFIEKF}$ and $\widehat{\mathbf{W}}_p^{RFIEKF}$	Tikhonov regularized Kalman gain, regularized state vector and regularized error covariance matrix respectively at p^{th} time instant.
$\hat{\mathbf{x}}_p^{CRFIEKF}$	Constraint Tikhonov regularized state vector at p^{th} time instant.
η and \varkappa	Number of constraints and number of state components of the extended state space model respectively.
\mathbf{k}^{final} and \mathbf{x}^{final}	Final values of states and estimated parameter.

2. Parameter estimation of Generic branch pathway model¹

We have examined a generic branched pathway model¹ (depicted in Supplementary Figure S1) encompassing five molecules and fourteen associated kinetic parameters, with six of these parameters remaining unknown. To tackle this, we devised a Fuzzy Inference System (FIS) aimed at capturing well-established approximate relationships among these molecules, as indicated by activation and inhibition interactions in Supplementary Figure S1. Detailed reaction fluxes and the stoichiometric matrix are presented in Supplementary Table S2-S3.

To facilitate the application of CRFIEKF for parameter estimation, we inferred the known imprecise relationships based on expert knowledge. These relationships are outlined in Supplementary Table S4-S5. Subsequently, we employed the proposed method to estimate the unknown parameter values. The results revealed that the majority of the estimated parameter values (enumerated in Supplementary Table S6) closely align with previous findings^{1,2}. The marginal differences between the estimated parameter values in our approach and those from prior methods underscore the effectiveness of our proposed technique. A visual representation of the comparison is presented in Supplementary Figure S2.

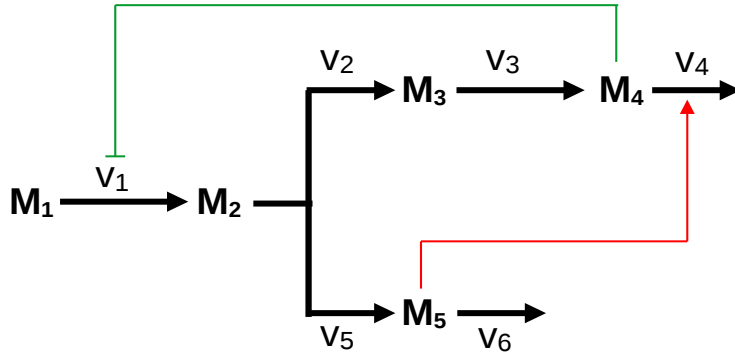


Figure S1. A generic branched pathway presented in Jia et al.¹

Table S2. Reaction equations 1. It contains the list of equations of reaction fluxes presented in Jia et al.¹

-
1. $v_1 = \frac{\gamma_1 M_1}{M_3^{f_{13}}}$
 2. $v_2 = \gamma_2 M_2^{f_{21}}$
 3. $v_3 = \gamma_3 M_3^{f_{32}}$
 4. $v_4 = \gamma_4 M_4^{f_{43}} M_5^{f_{44}}$
 5. $v_5 = \gamma_5 M_2^{f_{51}}$
 6. $v_6 = \gamma_6 M_5^{f_{64}}$
-

Table S3. It contains the stoichiometric matrix associated with the reactions from generic branch pathway model¹ under consideration.

	v1	v2	v3	v4	v5	v6
M1	1	-1	0	0	-1	0
M2	0	1	-1	0	0	0
M3	0	0	1	-1	0	0
M4	0	0	0	0	1	-1

Table S4. IF-THEN rule base for FIS to capture fuzzy relationship between M_2 , M_4 & M_3

IF (M_2 & M_4)		Then M_3
M_2	M_4	M_3
LOW	LOW	MEDIUM
LOW	MEDIUM	MEDIUM
LOW	HIGH	LOW
MEDIUM	LOW	MEDIUM
MEDIUM	MEDIUM	MEDIUM
MEDIUM	HIGH	LOW
HIGH	LOW	MEDIUM
HIGH	MEDIUM	LOW
HIGH	HIGH	HIGH

Table S5. IF-THEN rule base for FIS to capture fuzzy relationship between M_3 & M_1

IF M_3		Then M_1
M_3		M_1
LOW		HIGH
MEDIUM		MEDIUM
HIGH		LOW

Table S6. The list of parameter values of the generic branch pathway model¹. Here, we have estimated 7 parameter values (represented as “Estimated”) of the pathway under consideration. Rest of the parameter values (represented as “Known”) have been taken from previous investigation^{1,2}

Kinetic Parameter	Parameter values comparison				Status
	Void and Almeida, 2004	Jia et al.	CRFIEKF		
γ_1	20	19.9999	20		Known
γ_2	8	7.9998	8		Known
γ_3	3	2.9998	3		Known
γ_4	5	4.9998	5		Known
γ_5	2	2.0002	2		Known
γ_6	6	5.9997	6		Known
f_{13}	0.8	0.8	0.65		Estimated
f_{21}	0.5	0.5	0.40		Estimated
f_{32}	0.75	0.75	0.85		Estimated
f_{43}	0.5	0.5	0.48		Estimated
f_{44}	0.2	0.2	0.23		Estimated
f_{51}	0.5	0.4999	0.38		Estimated
f_{64}	0.8	0.7999	0.09		Estimated

Table S7. The table represents the sensitivity matrix of the generic branch pathway model with $m(=13)$ number of parameters. It represents the sensitivity of the output variables with respect to changes in the values of the parameters. In MATLAB, we determined the rank of the matrix to be 13. This result indicates that the sensitivity matrix is of full rank, suggesting that the model is identifiable based on the set of estimated parameter values.

0.40	0.99	0.00	0.54	1.07	0.08	0.31	0.03	0.11	0.00	0.11	0.04	0.03
1.05	0.22	1.34	1.43	2.83	0.23	0.81	0.09	0.02	0.72	0.30	0.10	0.07
1.92	1.27	0.00	2.62	5.20	1.33	1.49	0.17	0.14	0.00	0.55	0.59	0.13
0.08	0.21	0.00	0.12	0.23	0.22	0.42	0.01	0.02	0.00	0.02	0.10	0.04
11.47	19.69	36.43	70.10	135.24	21.52	38.64	0.94	2.39	18.52	14.45	10.10	3.47
28.14	83.42	568.40	42.93	82.61	19.88	23.64	2.48	15.55	75.70	8.82	9.34	2.13
24.32	3.18	100.64E2	29.46	56.91	3.77	16.24	221.87	0.37	0.50	6.10	1.66	1.46
10.44	22.03	9.50	5.40	56.46	0.76	5.38	0.92	2.69	2.09	6.17	0.27	0.48
5.74	12.25	0.23	6.93	13.37	13.00	3.10	2.56	1.47	0.12	1.43	6.20	4.39
7.61	11.44	36.26	65.44	126.22	29.19	43.79	1.28	1.40	18.43	13.49	10.33	3.94
9.53	20.35	11.84	16.63	32.10	3.04	9.19	0.80	2.57	3.17	3.42	1.44	0.82
17.56	36.38	1.18	20.80	40.31	9.79	11.54	1.59	4.55	0.48	4.36	4.97	2.89
1.26	12.99	6.62	1.55	3.05	28.27	0.87	0.11	1.54	3.27	0.33	5.49	0.08
18.42	48.39	5.45	21.81	42.30	18.39	10.98	1.67	5.99	2.79	4.57	10.50	2.84
4.77	11.12	3.86	33.59	86.05	12.62	24.50	0.37	1.46	10.92	9.32	6.07	2.23
11.29	27.88	62.38	84.02	161.72	28.96	46.25	1.02	3.28	21.90	17.28	13.52	4.16
8.40	17.90	1846.39	16.38	34.41	10.01	21.23	0.74	2.16	177.47	5.01	4.74	1.93

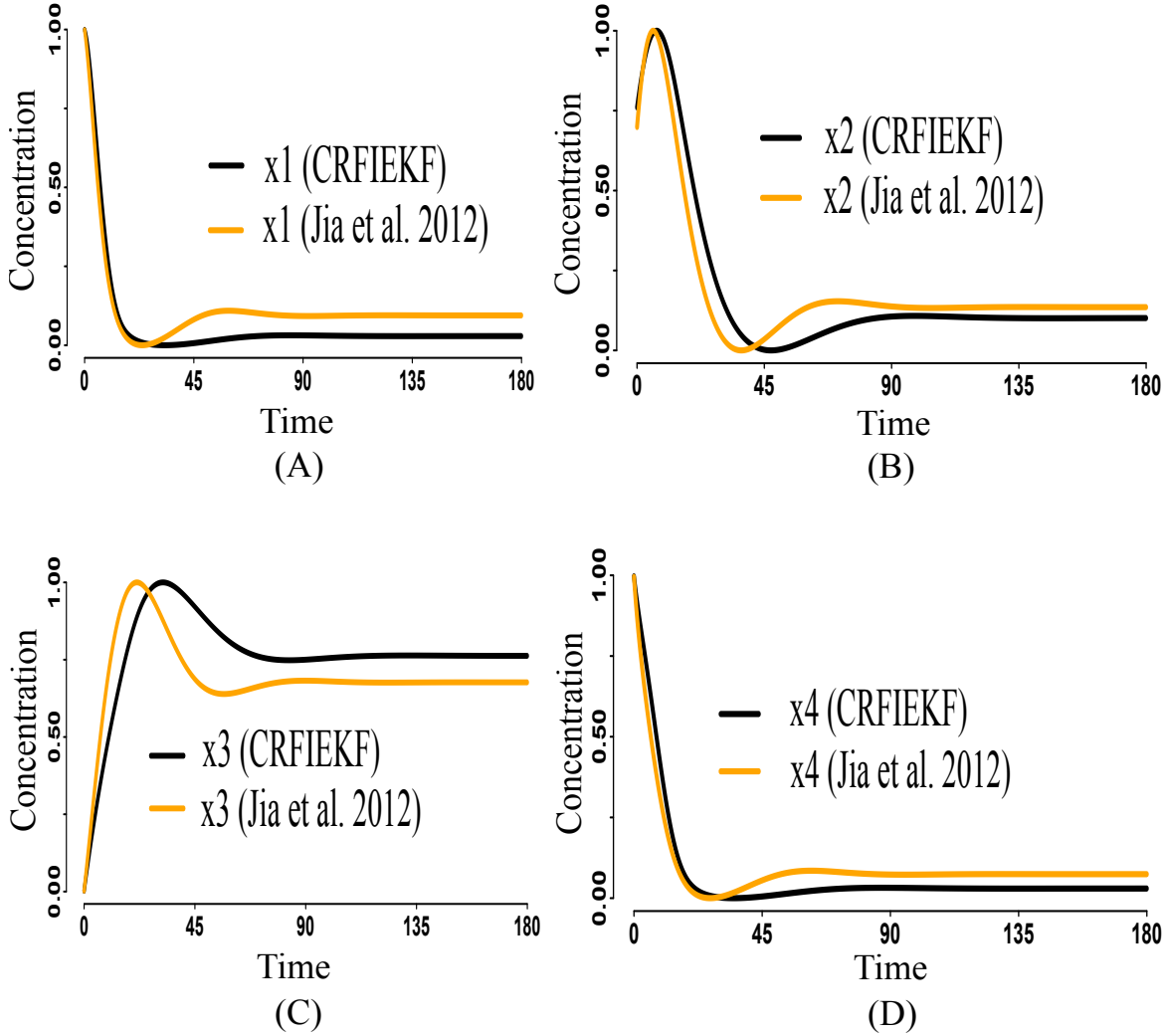


Figure S2. The figure illustrates the comparison of dynamics of x_1 , x_2 , x_3 and x_4 of general branch pathway model using proposed method as well as by Jia et al.¹

Table S8. The table represents the correlation coefficient of the parameter values of the generic branch pathway model¹. The rows and columns represents the set of kinetic parameters involved in the pathway. The correlation matrix having more than 60% absolute value < 0.5 signify that the model is distinguishable based on estimated parameter values.

	f_{13}	f_{21}	f_{32}	f_{43}	f_{44}	f_{51}	f_{64}	g_1	g_2	g_3	g_4	g_5	g_6
f_{13}	1.00												
f_{21}	-0.71	1.00											
f_{32}	0.35	-0.48	1.00										
f_{43}	-0.25	-0.12	-0.60	1.00									
f_{44}	0.20	0.23	0.58	-0.94	1.00								
f_{51}	0.13	-0.50	0.26	0.39	-0.34	1.00							
f_{64}	-0.12	0.36	0.35	-0.79	0.68	-0.43	1.00						
g_1	-0.36	0.50	-1.00	0.59	-0.58	-0.27	-0.34	1.00					
g_2	0.40	-0.92	0.49	0.27	-0.37	0.61	-0.37	-0.50	1.00				
g_3	-0.33	0.64	-0.96	0.38	-0.33	-0.42	-0.19	0.96	-0.70	1.00			
g_4	-0.19	-0.24	-0.57	0.94	-1.00	0.35	-0.69	0.57	0.39	0.32	1.00		
g_5	0.66	-0.37	0.33	-0.56	0.44	-0.51	0.24	-0.34	0.10	-0.24	-0.44	1.00	
g_6	-0.09	-0.16	0.83	-0.45	0.50	0.33	0.33	-0.83	0.31	-0.80	-0.49	-0.12	1.00

3. Parameter estimation of Mammalian glycolysis pathway

Glycolysis, a metabolic pathway, plays a fundamental role in converting glucose into pyruvate through a series of biochemical reactions, releasing a substantial amount of energy in the form of ATP and NADH molecules^{3,4}. Under normoxia conditions, most of the pyruvate molecules are utilized in the TCA cycle to initiate oxidative phosphorylation, resulting in lower lactate production compared to hypoxia. The interactions among the molecules involved in this pathway are illustrated in Supplementary Figure S3. To construct the state-space model of the pathway, we employed a modified version of the Michaelis-Menten equation⁵. This formulation introduces various unknown kinetic parameters, including catalytic rate constants, Michaelis rate constants, and feedback constants. In our study, we focused on 22 reactions of the pathway, obtained from KEGG⁶, and presented in Supplementary Table S9-S11, which detail the biochemical reactions, equations of reaction fluxes, and the stoichiometric matrix.

The state-space model encompasses a total of 47 kinetic parameters. Our approach, unlike previous methods, does not rely on prior knowledge of time-course experimental measurements. Instead, we generated an approximated measurement using a fuzzy inference system (FIS) based on known imprecise relationships among 15 metabolites and enzymes, as outlined in Supplementary Table S12, Supplementary Table S13-S16. The universe of discourse for the metabolites and enzymes was assumed to be within the range [0, 1]. Subsequently, we estimated the parameter values while varying the regularization techniques (Tikhonov, l_1 , and a hybrid of both), membership functions (Gaussian, Generalized Bell, Triangular, and Trapezoidal) of the FIS blocks, and the number of approximated measurements. The dynamics of eight metabolites (Glucose 6 phosphate, Fructose 6 phosphate, Fructose 1,6 bisphosphate, Dihydroxyacetone phosphate, 3 phosphoglycerate, Phosphoenol pyruvate, Pyruvate, and Lactate) in hypoxia-induced mammalian erythrocytes were observed using these estimated parameter values. The perturbed activities of these metabolites are presented in Supplementary Figure S4-S5, and the corresponding MSEs are summarized in Supplementary Table S17-S18. Interestingly, we found that the dynamics of the metabolites did not significantly differ across various settings, indicating that any regularization technique and membership function can be effectively employed in the estimation process. For our methodology, we chose Tikhonov regularization and Gaussian membership functions.

Additionally, we estimated the same set of parameter values using the approach of Lillacci et al.⁷, utilizing capillary electrophoresis mass spectrometry (CE-MS) measured concentration values⁸ (normalized in [0, 1]) associated with hypoxia-induced human erythrocytes as the measurement signal. Subsequently, we assessed the perturbed activities of eight metabolites in the glycolysis pathway of hypoxia-induced human erythrocytes, individually using the parameter values estimated by our proposed method and the previous investigation⁷. It should be noted that the activities of several related enzymes need to be modified, as evidenced by Kinoshita et al.⁸. We then compared the resulting behavior of these eight metabolites with the findings from the previous in silico/in vitro investigation⁸. Remarkably, the MSEs of the dynamics of these metabolites using our proposed method, Lillacci et al.⁷, and Kinoshita et al.⁸ were found to be significantly close ($p < 0.001$), highlighting the effectiveness of our approach. Supplementary Figure S7-S8 depict the perturbed activity of these metabolites.

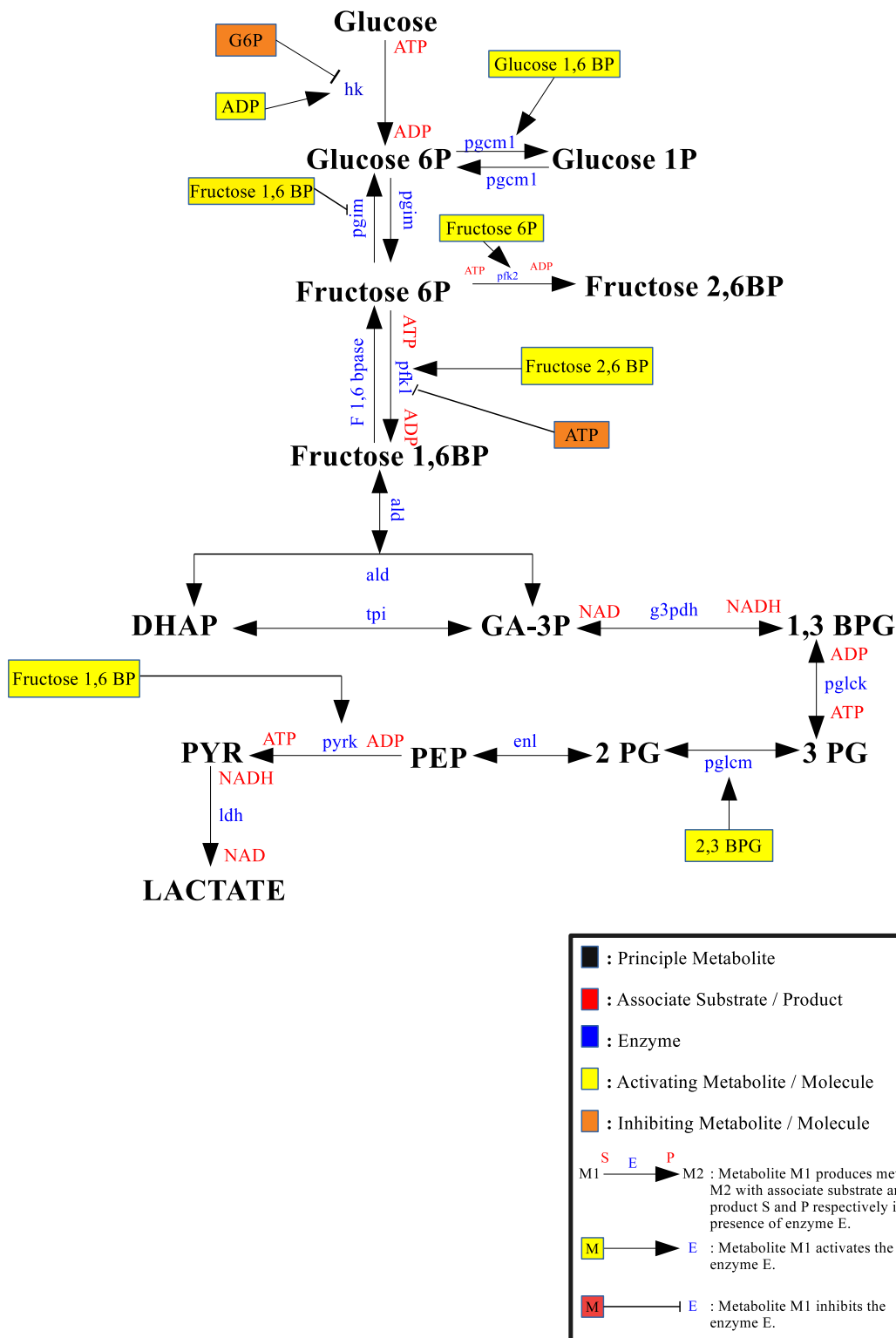


Figure S3. This figure depicts reduced glycolysis pathway under consideration. We have considered 22 reactions of the pathway collected from KEGG⁶

Table S9. Reaction list 2. It contains the list of 22 reactions from KEGG database for mammalian glycolysis pathway under consideration. Here the reaction numbers correspond to the same serial numbers in table* S7.

-
1. Glucose + ATP \Rightarrow Glucose 6-phosphate + ADP
 2. Glucose 6-phosphate \Rightarrow Glucose
 3. Glucose 6-phosphate \Rightarrow Fructose 6-phosphate
 4. Fructose 6-phosphate \Rightarrow Glucose 6-phosphate
 5. Fructose 6-phosphate + ATP \Rightarrow Fructose 1,6-bisphosphate + ADP
 6. Fructose 1,6-bisphosphate \Rightarrow Fructose 6-phosphate
 7. Fructose 6-phosphate + ATP \Rightarrow Fructose 2,6-bisphosphate + ADP
 8. Fructose 2,6-bisphosphate \Rightarrow Fructose 6-phosphate
 9. Fructose 1,6BP \Rightarrow Dihydroxyacetone phosphate + Glyceraldehyde 3-phosphate
 10. Dihydroxyacetone phosphate + Glyceraldehyde 3-phosphate \Rightarrow Fructose-1,6BP
 11. Dihydroxyacetone phosphate \Rightarrow Glyceraldehyde 3-phosphate
 12. Glyceraldehyde 3-phosphate \Rightarrow Dihydroxyacetone phosphate
 13. Glyceraldehyde 3-phosphate + NAD \Rightarrow 1,3-Bisphosphoglycerate + NADH
 14. 1,3-Bisphosphoglycerate + NADH \Rightarrow Glyceraldehyde 3-phosphate + NAD
 15. 1,3-Bisphosphoglycerate + ADP \Rightarrow 3-Phosphoglycerate + ATP
 16. 3-Phosphoglycerate \Rightarrow 1,3-Bisphosphoglycerate
 17. 3-Phosphoglycerate \Rightarrow 2-Phosphoglycerate
 18. 2-Phosphoglycerate \Rightarrow 3-Phosphoglycerate
 19. 2-Phosphoglycerate \Rightarrow Phosphoenolpyruvate
 20. Phosphoenolpyruvate \Rightarrow 2-Phosphoglycerate
 21. Phosphoenolpyruvate + ADP \Rightarrow Pyruvate + ATP
 22. Pyruvate + NADH \Rightarrow Lactate + NAD
-

Table S10. Reaction equations 2. It contains the list of equations of reaction fluxes associated with 22 reactions from KEGG database for mammalian glycolysis pathway under consideration. Here the serial numbers correspond to the same reaction numbers in Table S6.

1.	$v_1 = \frac{((K_{hexokinase} \cdot [hexokinase] \cdot [glucose] \cdot [ATP]) \cdot (1 + F_1 \cdot [ADP]))}{(Km_1 + [glucose] \cdot [ATP]) \cdot (1 + F_2 \cdot [glucose6P])}$
2.	$v_2 = \frac{(K_{glucose6Pase} \cdot [glucose6Pase] \cdot [glucose6P] \cdot (1 + F_3 \cdot [glucose6P]))}{(km_2 + [glucose6P])}$
3.	$v_3 = \frac{(k_{phosphoglucoisomerase} \cdot [phosphoglucoisomerase] \cdot [glucose6P])}{((Km_3 + [glucose6P]) \cdot (1 + F_4 \cdot [fructose1,6BP]))}$
4.	$v_4 = \frac{(K_{phosphoglucoisomerase} \cdot [phosphoglucoisomerase] \cdot [fructose6P])}{((Km_4 + [fructose6P]) \cdot (1 + F_5 \cdot [fructose1,6BP]))}$
5.	$v_5 = \frac{((K_{phosphofructokinase1} \cdot [phosphofructokinase1] \cdot [fructose6P] \cdot [ATP]) \cdot (1 + F_6 \cdot [f_26BP]))}{((Km_5 + [fructose6P] \cdot [ATP]) \cdot (1 + F_7 \cdot [ATP]))}$
6.	$v_6 = \frac{(K_{fructose1,6Bpase} \cdot [fructose1,6Bpase] \cdot [fructose1,6BP])}{((Km_6 + [fructose1,6BP]) \cdot (1 + F_8 \cdot [fructose2,6BP]))}$
7.	$v_7 = \frac{((K_{phosphofructokinase2} \cdot [phosphofructokinase2] \cdot [fructose6P] \cdot [ATP]) \cdot (1 + F_9 \cdot [fructose6P]))}{((Km_7 + [fructose6P] \cdot [ATP]))}$
8.	$v_8 = \frac{((K_{fructose2,6Bpase} \cdot [fructose2,6Bpase] \cdot [fructose2,6BP])}{((Km_8 + [fructose2,6BP]) \cdot (1 + F_{10} \cdot [fructose6P]))}$
9.	$v_9 = \frac{(K_{aldolase} \cdot [aldolase] \cdot [fructose1,6BP])}{(Km_9 + [fructose1,6BP])}$
10.	$v_{10} = \frac{(K_{aldolase} \cdot [aldolase] \cdot [dihydroxyacetonephosphate] \cdot [glyceraldehyde3P])}{(Km_{10} + [dihydroxyacetonephosphate] \cdot [glyceraldehyde3P])}$
11.	$v_{11} = \frac{(K_{triosephosphateisomerase} \cdot [triosephosphateisomerase] \cdot [dihydroxyacetonephosphate])}{(Km_{11} + [dihydroxyacetonephosphate])}$
12.	$v_{12} = \frac{(K_{triosephosphateisomerase} \cdot [triosephosphateisomerase] \cdot [glyceraldehyde3P])}{(Km_{12} + [glyceraldehyde3P])}$
13.	$v_{13} = \frac{(K_{Glyceraldehyde3Pdehydrogenase} \cdot [Glyceraldehyde3Pdehydrogenase] \cdot [glyceraldehyde3P] \cdot [NAD])}{(Km_{13} + [glyceraldehyde3P] \cdot [NAD])}$
14.	$v_{14} = \frac{(K_{Glyceraldehyde3Pdehydrogenase} \cdot [Glyceraldehyde3Pdehydrogenase] \cdot [1,3bisphosphoglycerate] \cdot [NADH])}{(Km_{14} + [1,3bisphosphoglycerate] \cdot [NADH])}$
15.	$v_{15} = \frac{(K_{Phosphogluokinase} \cdot [Phosphoglucoisomerase] \cdot [1,3bisphosphoglycerate] \cdot [ADP])}{(Km_{15} + [1,3bisphosphoglycerate] \cdot [ADP])}$
16.	$v_{16} = \frac{(K_{Phosphogluokinase} \cdot [Phosphoglucoisomerase] \cdot [3phosphoglycerate])}{(Km_{16} + [3phosphoglycerate])}$
17.	$v_{17} = \frac{((K_{phosphoglucomutase} \cdot [phosphoglucomutase] \cdot [3phosphoglycerate]) \cdot (1 + F_{24} \cdot [2,3bisphosphoglycerate]))}{(Km_{17} + [3phosphoglycerate])}$
18.	$v_{18} = \frac{((K_{phosphoglucomutase} \cdot [phosphoglucomutase] \cdot [2phosphoglycerate]) \cdot (1 + F_{25} \cdot [2,3bisphosphoglycerate]))}{(Km_{18} + [2phosphoglycerate])}$
19.	$v_{19} = \frac{(K_{enolase} \cdot [enolase] \cdot [2phosphoglycerate])}{(Km_{19} + [2phosphoglycerate])}$
20.	$v_{20} = \frac{(K_{enolase} \cdot [enolase] \cdot [phosphoenolpyruvate])}{(Km_{20} + [phosphoenolpyruvate])}$
21.	$v_{21} = \frac{((K_{pyruvatekinase} \cdot [pyruvatekinase] \cdot [phosphoenolpyruvate] \cdot [ADP]) \cdot (1 + F_{11} \cdot [fructose1,6BP]))}{((Km_{21} + [phosphoenolpyruvate] \cdot [ADP]) \cdot (1 + F_{12} \cdot [ATP]))}$
22.	$v_{22} = \frac{(K_{lactatedehydrogenase} \cdot [lactatedehydrogenase] \cdot [pyruvate] \cdot [NADH])}{(Km_{22} + [pyruvate] \cdot [NADH])}$

Table S11. It contains the stoichiometric matrix associated with 22 reactions from KEGG database for mammalian glycolysis pathway under consideration. The rows represent the metabolites involved in the pathway where as the columns represent fluxes associated with each reaction.

	v1	v2	v3	v4	v5	v6	v7	v8	v9	v10	v11	v12	v13	v14	v15	v16	v17	v18	v19	v20	v21	v22
Glucose 6 phosphate	1	-1	-1	0	0	0	0	0	0	0	0	0	0	0	0	0	0	0	0	0	0	
Glucose	-1	1	0	0	0	0	0	0	0	0	0	0	0	0	0	0	0	0	0	0	0	
Fructose 6 phosphate	0	0	1	-1	1	-1	1	0	0	0	0	0	0	0	0	0	0	0	0	0	0	
Fructose 1,6 Bisphosphate	0	0	0	0	1	-1	0	0	-1	1	0	0	0	0	0	0	0	0	0	0	0	
Fructose 2,6 Bisphosphate	0	0	0	0	0	0	1	-1	0	0	0	0	0	0	0	0	0	0	0	0	0	
Dihydroxyacetone phosphate	0	0	0	0	0	0	0	0	1	-1	-1	1	0	0	0	0	0	0	0	0	0	
Glyceraldehyde 3-phosphate	0	0	0	0	0	0	0	0	1	-1	1	0	0	0	0	0	0	0	0	0	0	
1,3-Bisphosphoglycerate	0	0	0	0	0	0	0	0	0	0	0	1	-1	1	0	0	0	0	0	0	0	
3 phosphoglycerate	0	0	0	0	0	0	0	0	0	0	0	0	0	1	-1	1	0	0	0	0	0	
2 phosphoglycerate	0	0	0	0	0	0	0	0	0	0	0	0	0	0	0	1	-1	1	0	0	0	
Phosphoenol pyruvate	0	0	0	0	0	0	0	0	0	0	0	0	0	0	0	0	0	1	-1	0	0	
Pyruvate	0	0	0	0	0	0	0	0	0	0	0	0	0	0	0	0	0	0	0	1	-1	
Lactate	0	0	0	0	0	0	0	0	0	0	0	0	0	0	0	0	0	0	0	0	1	
ATP	-1	0	0	-1	0	-1	0	0	0	0	0	0	0	0	1	0	0	0	0	1	0	
ADP	1	0	0	1	0	1	0	0	0	0	0	0	0	0	-1	0	0	0	0	-1	0	
NADH	0	0	0	0	0	0	0	0	0	0	0	1	-1	0	0	0	0	0	0	-1	0	
NAD	0	0	0	0	0	0	0	0	0	0	0	-1	1	0	0	0	0	0	0	0	1	

Table S12. This table shows the names of 15 fuzzy molecules of the FIS, used to estimate parameter of glycolysis pathway.

	Input metabolite list	Output metabolite list
FIS 1	Glucose, Pyruvate kinase	Pyruvate
FIS 2	Hexokinase, ATP, Glucose	Glucose 6 Phosphate, ADP
FIS 3	Glyceraldehyde 3P, Glyceraldehyde 3P Dehydrogenase , NAD	1,3 bisphosphoglycerate, NADH
FIS 4	Fructose 6 Phosphate, Phosphofructokinase 1	Fructose 1,6 bisphosphate

Table S13. IF–THEN rule base for FIS to capture fuzzy relationship between glucose & pyruvate kinase & Pyruvate

IF (glucose & pyruvate kinase)		Then pyruvate
Glucose	pyruvate kinase	Pyruvate
LOW	LOW	LOW
LOW	MEDIUM	LOW
LOW	HIGH	MEDIUM
MEDIUM	LOW	LOW
MEDIUM	MEDIUM	MEDIUM
MEDIUM	HIGH	MEDIUM
HIGH	LOW	LOW
HIGH	MEDIUM	MEDIUM
HIGH	HIGH	HIGH

Table S14. IF–THEN rule base for FIS to capture fuzzy relationship between hexokinase & ATP & glucose and Glucose6 Phosphate & ADP

IF (hexokinase & ATP & glucose)			Then (Glucose 6 Phosphate & ADP)	
Hexokinase	ATP	Glucose	Glucose 6 Phosphate	ADP
LOW	LOW	LOW	LOW	HIGH
LOW	LOW	MEDIUM	LOW	HIGH
LOW	LOW	HIGH	MEDIUM	HIGH
LOW	MEDIUM	LOW	LOW	MEDIUM
LOW	MEDIUM	MEDIUM	MEDIUM	MEDIUM
LOW	MEDIUM	HIGH	MEDIUM	MEDIUM
LOW	HIGH	LOW	LOW	LOW
LOW	HIGH	MEDIUM	MEDIUM	LOW
LOW	HIGH	HIGH	MEDIUM	LOW
MEDIUM	LOW	LOW	LOW	HIGH
MEDIUM	LOW	MEDIUM	MEDIUM	HIGH
MEDIUM	LOW	HIGH	MEDIUM	HIGH
MEDIUM	MEDIUM	LOW	LOW	MEDIUM
MEDIUM	MEDIUM	MEDIUM	MEDIUM	MEDIUM
MEDIUM	MEDIUM	HIGH	MEDIUM	MEDIUM
MEDIUM	HIGH	LOW	LOW	LOW
MEDIUM	HIGH	MEDIUM	MEDIUM	LOW
MEDIUM	HIGH	HIGH	MEDIUM	LOW
HIGH	LOW	LOW	LOW	HIGH
HIGH	LOW	MEDIUM	MEDIUM	HIGH
HIGH	LOW	HIGH	MEDIUM	HIGH
HIGH	MEDIUM	LOW	LOW	MEDIUM
HIGH	MEDIUM	MEDIUM	MEDIUM	MEDIUM
HIGH	MEDIUM	HIGH	MEDIUM	MEDIUM
HIGH	HIGH	LOW	LOW	LOW
HIGH	HIGH	MEDIUM	MEDIUM	LOW
HIGH	HIGH	HIGH	HIGH	LOW

Table S15. IF–THEN rule base for FIS to capture fuzzy relationship between glyceraldehyde 3P & glyceraldehyde 3P deh & NAD and 1,3-BPG & NADH. Here, glyclrdh 3P, glyclrdh 3P deh, 1,3-BPG stands for glyceraldehyde 3 phosphate, glyceraldehyde 3 phosphate dehydrogenase and 1,3 Biphosphoglycerate respectively.

IF glyclrdh 3P & glyclrdh 3P deh & NAD			Then 1,3-BPG & NADH	
glyclrdh 3P	glyclrdh 3P deh	NAD	1,3-BPG	NADH
LOW	LOW	LOW	LOW	LOW
LOW	LOW	MEDIUM	LOW	MEDIUM
LOW	LOW	HIGH	LOW	MEDIUM
LOW	MEDIUM	LOW	LOW	LOW
LOW	MEDIUM	MEDIUM	LOW	MEDIUM
LOW	MEDIUM	HIGH	MEDIUM	MEDIUM
LOW	HIGH	LOW	LOW	LOW
LOW	HIGH	MEDIUM	LOW	MEDIUM
LOW	HIGH	HIGH	LOW	MEDIUM
MEDIUM	LOW	LOW	LOW	LOW
MEDIUM	LOW	MEDIUM	LOW	MEDIUM
MEDIUM	LOW	HIGH	MEDIUM	MEDIUM
MEDIUM	MEDIUM	LOW	MEDIUM	MEDIUM
MEDIUM	MEDIUM	MEDIUM	MEDIUM	MEDIUM
MEDIUM	MEDIUM	HIGH	MEDIUM	HIGH
MEDIUM	HIGH	LOW	MEDIUM	LOW
MEDIUM	HIGH	MEDIUM	MEDIUM	MEDIUM
MEDIUM	HIGH	HIGH	MEDIUM	HIGH
HIGH	LOW	LOW	LOW	LOW
HIGH	LOW	MEDIUM	LOW	MEDIUM
HIGH	LOW	HIGH	LOW	MEDIUM
HIGH	MEDIUM	LOW	MEDIUM	LOW
HIGH	MEDIUM	MEDIUM	MEDIUM	MEDIUM
HIGH	MEDIUM	HIGH	MEDIUM	HIGH
HIGH	HIGH	LOW	HIGH	LOW
HIGH	HIGH	MEDIUM	HIGH	MEDIUM
HIGH	HIGH	HIGH	HIGH	HIGH

Table S16. IF–THEN rule base for FIS to capture fuzzy relationship between Fructose 6P & Pfk1 & ATP and Fructose 1,6BP. Here, pfk1 stands for phosphofructokinase 1.

IF Fructose 6P & Pfk1 & ATP			Then Fructose 1,6BP
Fructose 6P	Pfk1	ATP	Fructose 1,6BP
LOW	LOW	LOW	LOW
LOW	LOW	MEDIUM	LOW
LOW	LOW	HIGH	LOW
LOW	MEDIUM	LOW	LOW
LOW	MEDIUM	MEDIUM	LOW
LOW	MEDIUM	HIGH	LOW
LOW	HIGH	LOW	LOW
LOW	HIGH	MEDIUM	LOW
LOW	HIGH	HIGH	LOW
MEDIUM	LOW	LOW	LOW
MEDIUM	LOW	MEDIUM	LOW
MEDIUM	LOW	HIGH	LOW
MEDIUM	MEDIUM	LOW	MEDIUM
MEDIUM	MEDIUM	MEDIUM	MEDIUM
MEDIUM	MEDIUM	HIGH	MEDIUM
MEDIUM	HIGH	LOW	LOW
MEDIUM	HIGH	MEDIUM	MEDIUM
MEDIUM	HIGH	HIGH	MEDIUM
HIGH	LOW	LOW	MEDIUM
HIGH	LOW	MEDIUM	MEDIUM
HIGH	LOW	HIGH	MEDIUM
HIGH	MEDIUM	LOW	MEDIUM
HIGH	MEDIUM	MEDIUM	MEDIUM
HIGH	MEDIUM	HIGH	HIGH
HIGH	HIGH	LOW	MEDIUM
HIGH	HIGH	MEDIUM	HIGH
HIGH	HIGH	HIGH	HIGH

Comparison of dynamics of 8 metabolites using proposed method considering Tikhonov, L1 and the combination of both regularization respectively and simulation result by Kinoshita et al.

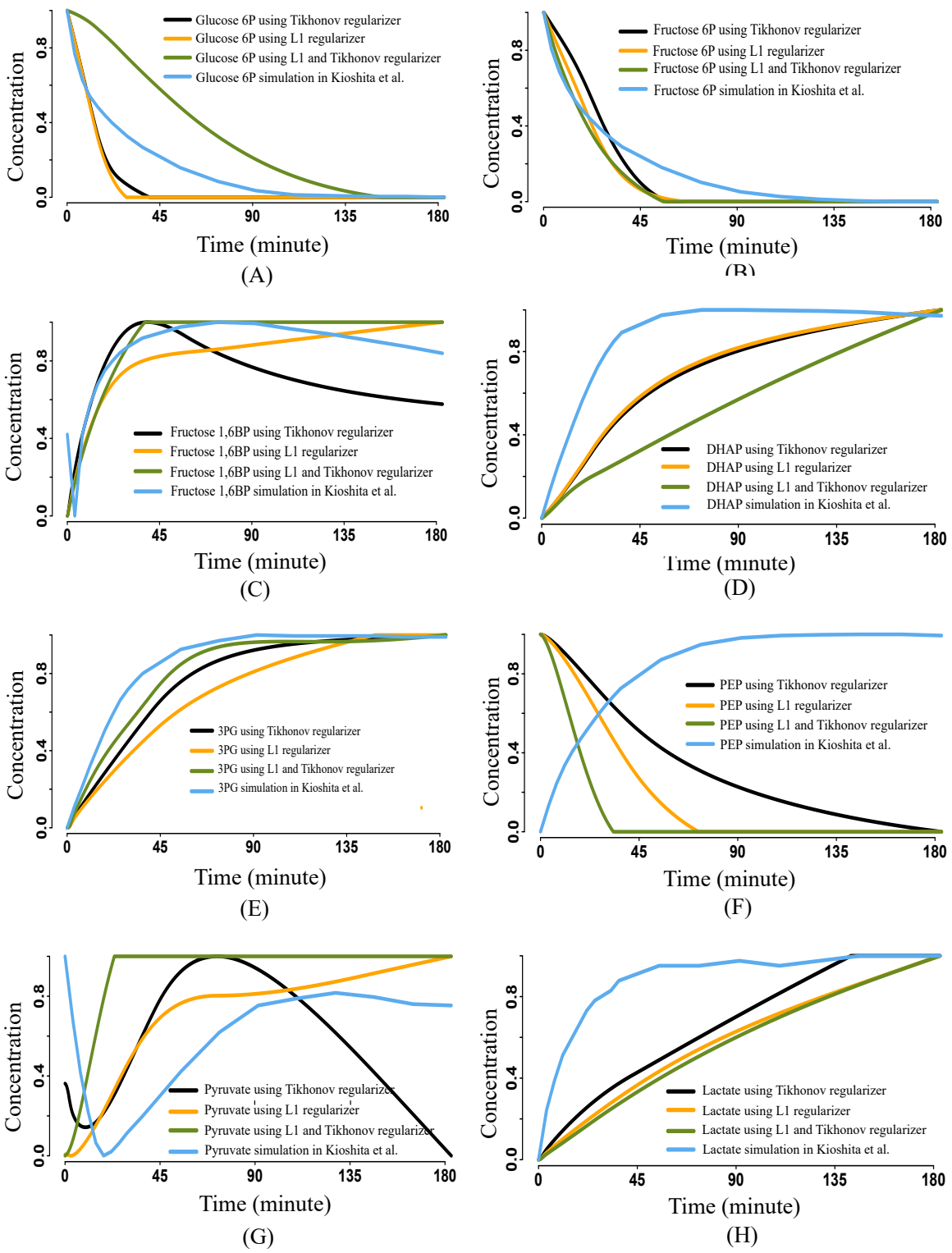


Figure S4. This figure demonstrates the dynamics of 8 metabolites during hypoxia using the parameter values estimated by the proposed method. Here, we have separately estimated the parameter values incorporating L1 regularization, Tikhonov regularization, and a combined L1 followed by Tikhonov regularization. Afterward, we have separately captured the perturbed activities of eight metabolites of the glycolysis pathway of hypoxia-induced human erythrocytes. We have observed that L1, as well as the Tikhonov regularized technique, have a similar influence on the dynamics of hypoxia-induced human erythrocytes⁸. However, incorporating the combination of L1 followed by the Tikhonov regularization slightly deviates the trajectories. The result confirms the effectiveness of employing Tikhonov regularization in the proposed technique.

Comparison of dynamics of 4 metabolites using proposed method, HEKF (Lillacci et al.(2010)) and simulation result by Kinoshita et al. (2007).

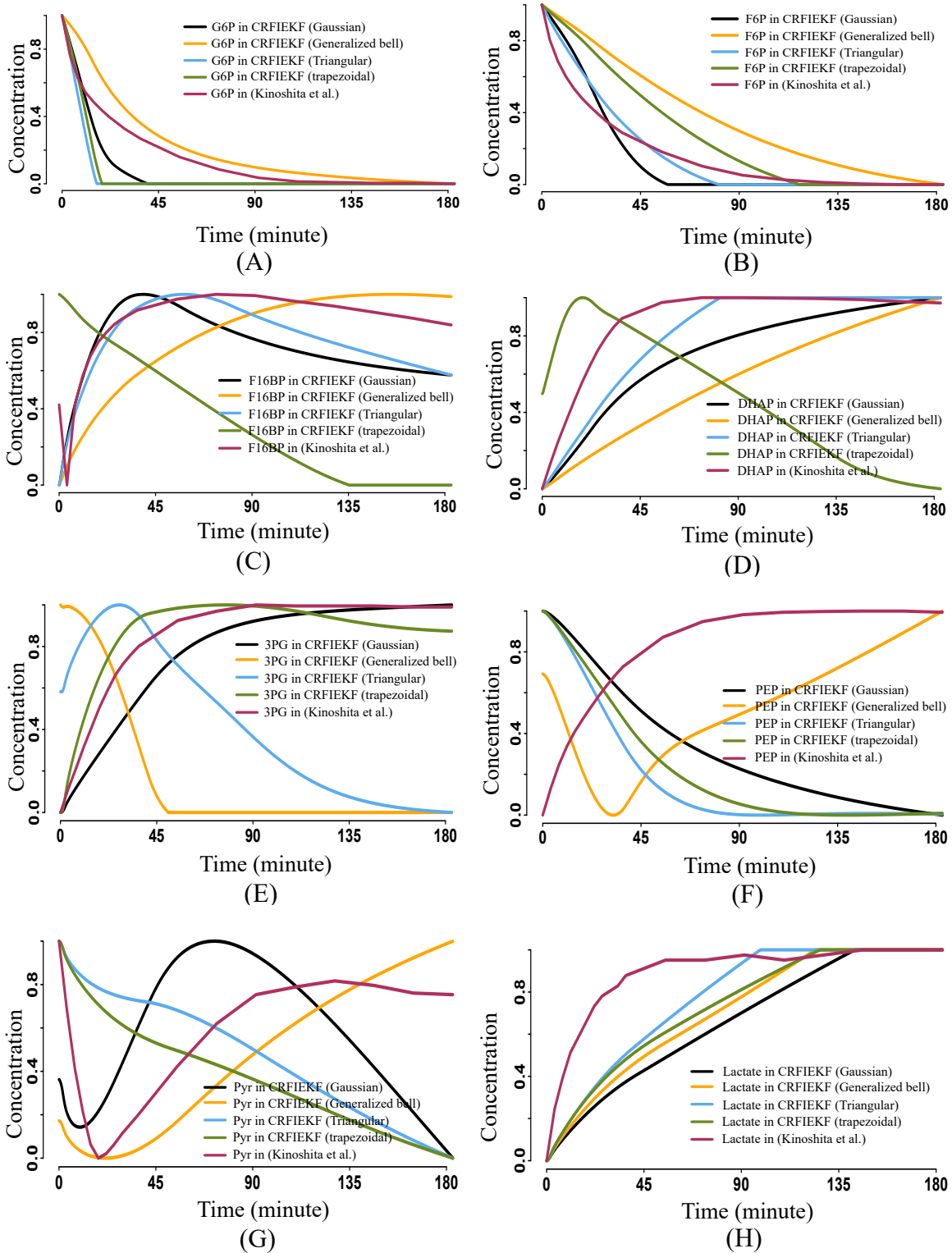


Figure S5. This figure demonstrates the dynamics of 8 metabolites during hypoxia using the parameter values estimated by proposed method. Here, we have separately estimated the parameter values considering Gaussian, Generalized bell, Triangular and Trapezoidal membership function in the FIS. Afterwards, we have separately captured the perturbed activities of eight metabolites of glycolysis pathway of hypoxia-induced human erythrocytes. We have obtained the most similar dynamics as Kinoshita et al.⁸, with the help of parameter values estimated by CRFIEKF having Gaussian membership function in the FIS. The result confirms the effectiveness of using Gaussian membership function in the investigation.

Table S17. This table demonstrates the MSE of dynamics of eight metabolites of hypoxia induced human erythrocytes in Kinoshita et al.⁸ and proposed technique using the parameter values considering Tikhonov regularization, l_1 regularization and a hybrid of them during parameter estimation process.

Metabolite	MSE comparison		
	Kinoshita et al. ⁸ vs CRFIEKF (Tokhonov regularized)	Kinoshita et al. ⁸ vs CRFIEKF (l_1 regularized)	Kinoshita et al. ⁸ vs CRFIEKF (combined regularized)
Glucose 6 phosphate	0.0150	0.0163	0.0213
Fructose 6 phosphate	0.0054	0.0056	0.0060
Fructose 1,6 bisphosphate	0.1506	0.0744	0.0113
Dihydroxyacetone phosphate	0.0488	0.0972	0.1721
3 Phosphoglycerate	0.1325	0.0148	0.2629
Phosphoenol pyruvate	0.4366	0.5865	0.6222
Pyruvate	0.0747	0.1184	0.2167
Lactate	0.0148	0.0292	0.0835

Table S18. This table demonstrates the MSE of dynamics of eight metabolites of hypoxia induced human erythrocytes in Kinoshita et al.⁸ and proposed technique using the parameter values considering membership function (MF) of the FIS block as Gaussian, Generalized Bell, Triangular and Trapezoidal during parameter estimation process.

Metabolite	MSE comparison			
	Kinoshita et al. ⁸ vs CRFIEKF (Gaussian MF)	Kinoshita et al. ⁸ vs CRFIEKF (Generalized Bell MF)	Kinoshita et al. ⁸ vs CRFIEKF (Triangular MF)	Kinoshita et al. ⁸ vs CRFIEKF (Trapezoidal MF)
Glucose 6 phosphate	0.0150	0.0180	0.0218	0.0193
Fructose 6 phosphate	0.0054	0.0529	0.0051	0.0223
Fructose 1,6 bisphosphate	0.1506	0.1094	0.1106	0.5015
Dihydroxyacetone phosphate	0.0488	0.1843	0.0092	0.2583
3 Phosphoglycerate	0.1325	0.6305	0.4312	0.1806
Phosphoenol pyruvate	0.4366	0.1007	0.3292	0.2527
Pyruvate	0.0747	0.0580	0.1158	0.1135
Lactate	0.0148	0.0115	0.0084	0.0098

Table S19. This table demonstrates the MSE of dynamics of eight metabolites of hypoxia induced human erythrocytes in Kinoshita et al.⁸ and proposed technique using the parameter values considering 4, 5, 6 approximated measurement based on known imprecise relationship among the molecules of the pathway during parameter estimation process.

Metabolite	MSE comparison		
	Kinoshita et al. ⁸ vs CRFIEKF (6 approximated measurement)	Kinoshita et al. ⁸ vs CRFIEKF (5 approximated measurement)	Kinoshita et al. ⁸ vs CRFIEKF (4 approximated measurement)
Glucose 6 phosphate	0.0150	0.0154	0.0154
Fructose 6 phosphate	0.0054	0.0386	0.0058
Fructose 1,6 bisphosphate	0.1506	0.0278	0.1051
Dihydroxyacetone phosphate	0.0488	0.1428	0.0458
3 Phosphoglycerate	0.1325	0.2254	0.4272
Phosphoenol pyruvate	0.4366	0.6138	0.3027
Pyruvate	0.0747	0.1552	0.0666
Lactate	0.0148	0.0084	0.0479

Comparison of dynamics of 8 metabolites using proposed method
considering 6, 5 and 4 approximate observation respectively
and simulation result by Kinoshita et al.

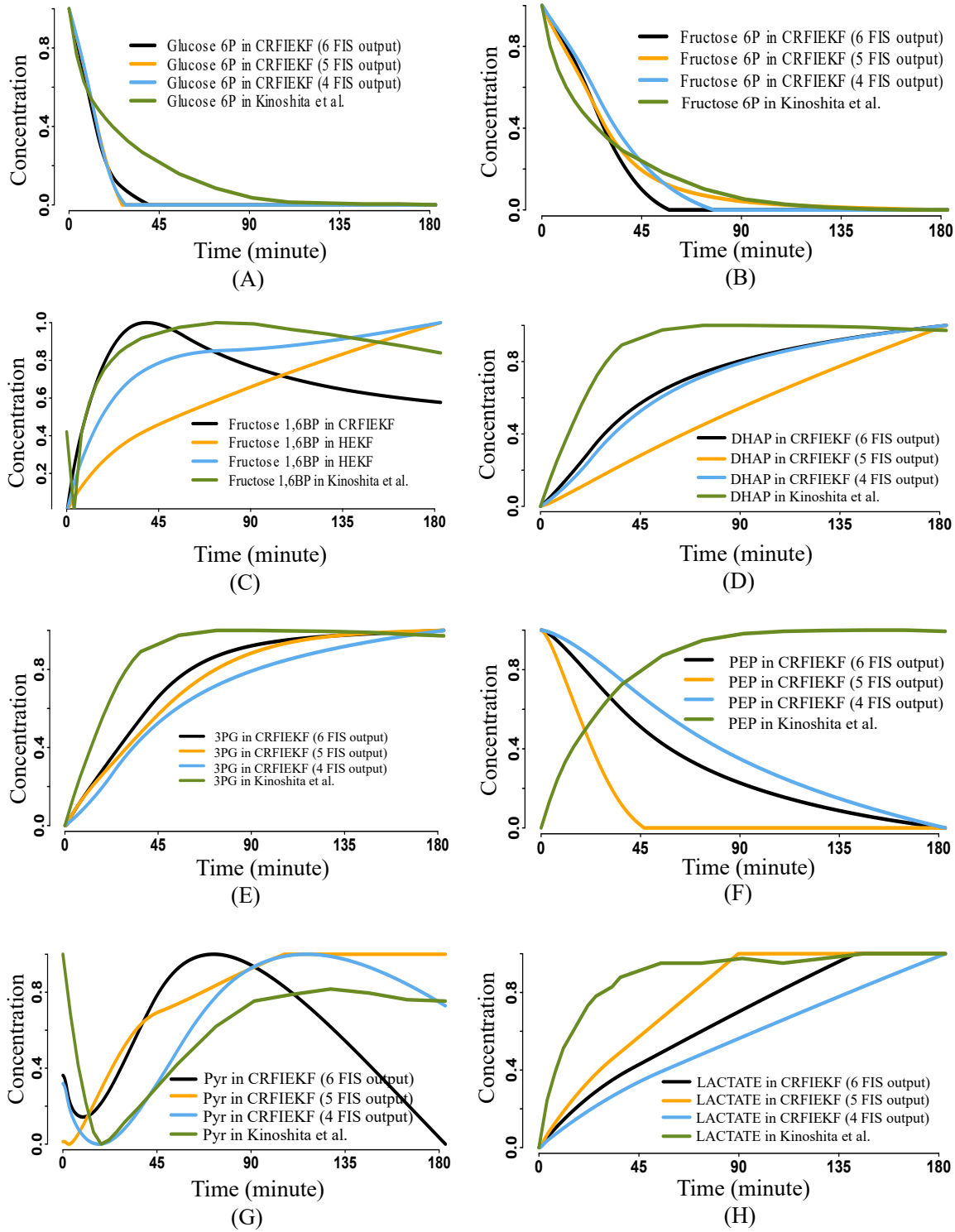


Figure S6. This figure demonstrates the dynamics of 8 metabolites during hypoxia using the parameter values estimated by proposed method. Here, we have separately estimated the parameter values assuming 6, 5 and 4 approximate observation from the FIS. Afterwards, we have separately captured the perturbed activities of eight metabolites of glycolysis pathway of hypoxia-induced human erythrocytes. In spite of altering the number of observations the dynamics shows almost similar behavior (The MSE for all the metabolites are not significantly different at $p < 0.001$.) as the simulation result by Kinoshita et al.⁸. This result clearly validate the robustness of the proposed methodology.

Table S20. (A) We have separately estimated the parameter values by altering the regularization technique in the proposed method. Afterwards, using the parameter values for each of three regularization techniques, such as Tikhonov, l_1 and a hybrid of both, we have evaluated the MSEs of the dynamics of eight metabolites of hypoxia-induced human erythrocytes based on the simulation result and CE-MS measurement (normalized in [0, 1])⁸. In this way, we have developed two cases where each case comprises three sets of MSEs of eight metabolites corresponding to three regularization techniques. On performing ANOVA test among the three sets of MSEs in both cases, we have observed that the F-statistic value < F-critical value. Such a result represents that the regularization techniques have no significantly different influence on the parameter estimation techniques. In (B), we have obtained the MSE of eight metabolites in a similar way as mentioned in (A) using parameter values estimated by altering Gaussian, Generalized bell, Triangular and Trapezoidal membership function distinctly. Unlike (A) here each case comprises four sets of MSEs of eight metabolites corresponding to four membership functions. We have further noticed that F-statistic value < F-critical value in both cases. Such result indicates that the proposed technique does not generate significantly different results on altering membership function. Finally, in (C), similar to aforementioned cases, altering number of approximated observations (four/five/six), each of the two cases comprises three sets of MSEs corresponding to the number of approximated observations. In this case also we have observed F-statistic value < F-critical value. Such result supports the claim of robustness of the estimation technique. Here, all the claims have been considered at 95% significance level. The column name “F-stat” and “F-crit” represent “F-statistics” and “F-critical” respectively.

Type	ANOVA test result			
	MSE based on	F-stat	P-value	F-crit
A. Regularization comparison	<i>in silico</i> simulation	0.2973	0.7459	3.4668
	CE-MS measurement	0.8195	0.4543	3.4668
B. Membership function comparison	<i>in silico</i> simulation	0.1772	0.911	2.9467
	CE-MS measurement	0.4161	0.7428	2.9467
C. Number of measurement comparison	<i>in silico</i> simulation	0.1365	0.8732	3.4668
	CE-MS measurement	1.0906	0.3543	3.4668

Table S21. This table depicts the initial value and estimated value of 47 parameters in glycolysis pathway.

Constant type	Parameter name	Initial value	Estimated value
Michaelis menten constant	km_1	0.052076	0.713900953
	km_2	0.4479	0.295157569
	km_3	0.052373	0.999467309
	km_4	0.4289	0.559038695
	km_5	0.054248	0.881503044
	km_6	0.4654	0.150000318
	km_7	0.053261	0.857460471
	km_8	0.07412	0.101167381
	km_9	0.1	0.426330857
	km_{10}	0.4415	0.632187475
	km_{11}	0.09692	0.9999
	km_{12}	0.7	0.815084321
	km_{13}	0.051036	0.968071306
	km_{14}	0.4729	0.445439606
	km_{15}	0.2	0.122681749
	km_{16}	0.4658	0.660009019
	km_{17}	0.053377	0.770427701
	km_{18}	0.3951	0.100012031
	km_{19}	0.073413	0.599673996
	km_{20}	0.42947	0.71799882
	km_{21}	0.13745	0.957762128
	km_{22}	0.7	0.233415694
Kinatic rate constant	$K_{hexokinase}$	0.02	0.673164996
	$K_{glucose6Pase}$	0.05	0.928702688
	$K_{phosphoglucoisomerase}$	0.0812	0.97646051
	$K_{phosphofructokinase1}$	0.09	0.968551348
	$K_{phosphofructokinase2}$	0.09	0.749009801
	$K_{aldolase}$	0.0826	0.485551038
	$K_{triosephosphateisomerase}$	0.0899	0.990298839
	$K_{Glyceraldehyde3Pdehydrogenase}$	0.01	0.672711844
	$K_{Phosphoglucokinase}$	0.0532	0.569340445
	$K_{phosphoglucomutase}$	0.06	0.299129342
	$K_{enolase}$	0.0727	0.100009938
	$K_{pyruvatekinase}$	0.2	0.833384647
	$K_{lactatedehydrogenase}$	0.01	0.669398944
	F_1	0.5	0.847604148
Feedback constant	F_2	0.5	0.853760185
	F_3	0.5	0.814920604
	F_4	0.5	0.206016679
	F_5	0.5	0.89288036
	F_6	0.5	0.168305091
	F_7	0.5	0.966223314
	F_8	0.5	0.50000004
	F_9	0.5	0.169828564
	F_{10}	0.5	0.50000004
	F_{11}	0.5	0.904357963
	F_{12}	0.5	0.466043176

Comparison of dynamics of 4 metabolites using proposed method, HEKF (Lillacci et al.(2010)) and simulation result by Kinoshita et al. (2007).

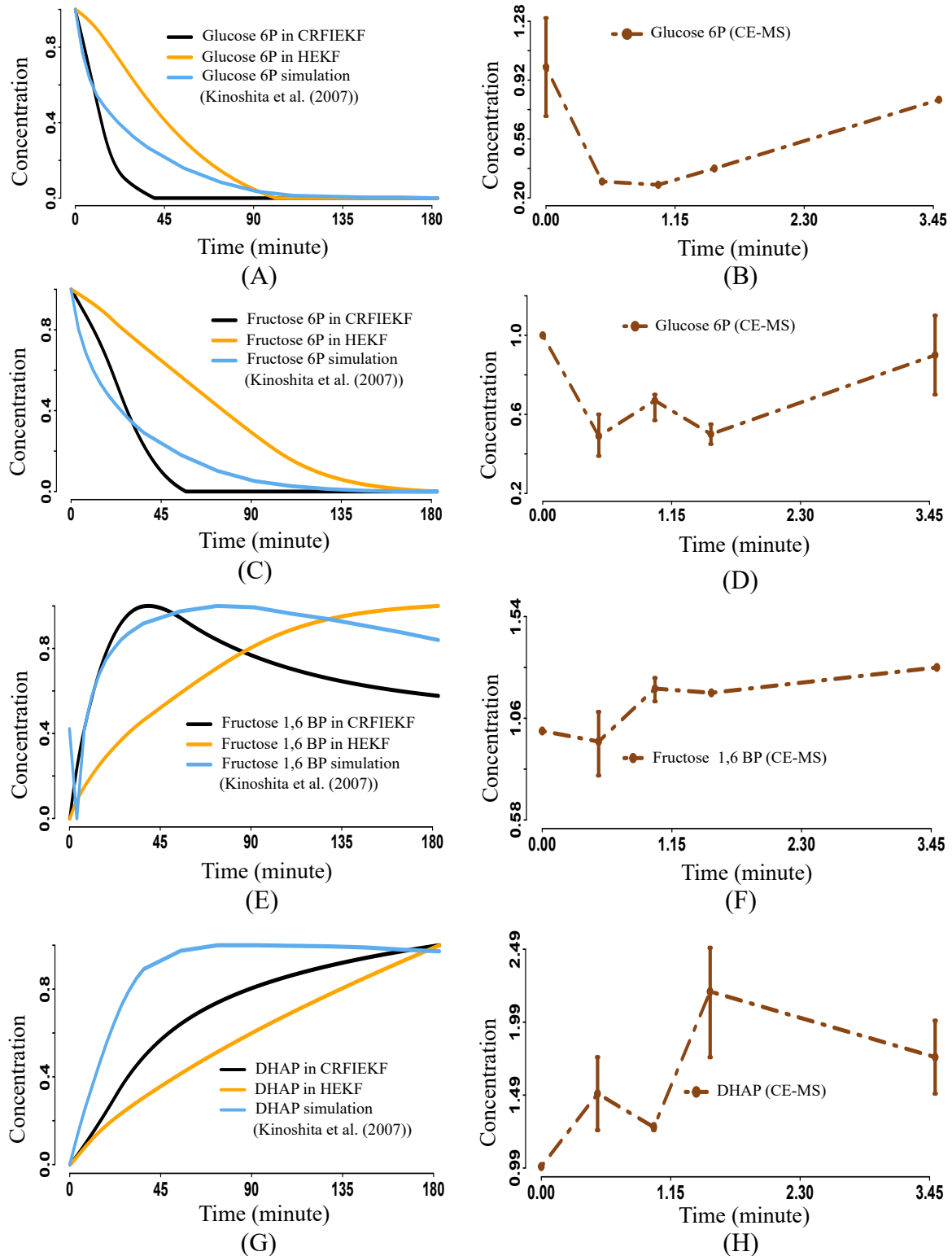


Figure S7. Validation of the proposed model during hypoxia through CE-MS measurement and simulation in human erythrocytes (Kinoshita et al.⁸).

Comparison of dynamics of 4 metabolites using proposed method, HEKF (Lillacci et al.(2010)) and simulation result by Kinoshita et al. (2007).

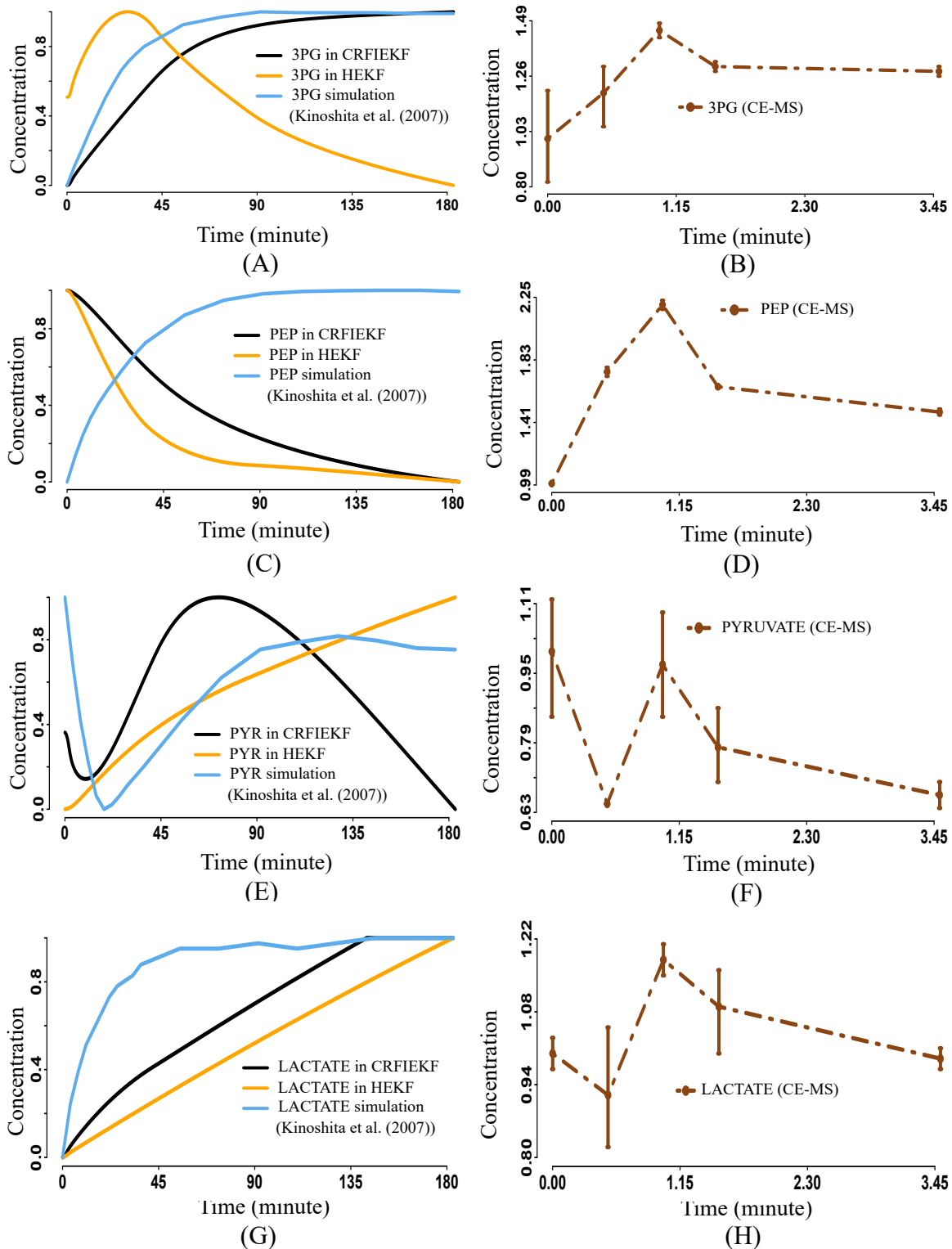


Figure S8. Validation of the proposed model during hypoxia through CE-MS measurement and simulation in human erythrocytes (Kinoshita et al.⁸).

4. Parameter estimation of anaerobic glycolysis pathway in a yeast cell⁹

The model is depicted in Supplementary Figure S9. It comprise of seven metabolites and thirteen associated kinetic parameters. The list of reactions has been presented in Supplementary Table S22. Moreover, the dynamics of the molecules has been expressed using ordinary differential equation in Supplementary Table S23. We have utilized the known approximate relationship among some of the molecules of the pathway to evaluate the parameter values using proposed technique. We have demonstrated such known approximate relationship in Supplementary Table S24-S25. Afterwards, we have revealed the dynamics of the molecules (Normalized in [0, 1]) of the pathway using the parameter values estimated by proposed technique as well as previous investigations^{9,10}. The MSE (illustrated in Supplementary Table S26) between resultant concentrations of the seven metabolites by the proposed methods with time and the corresponding simulation signifies the potential of the proposed methodology.

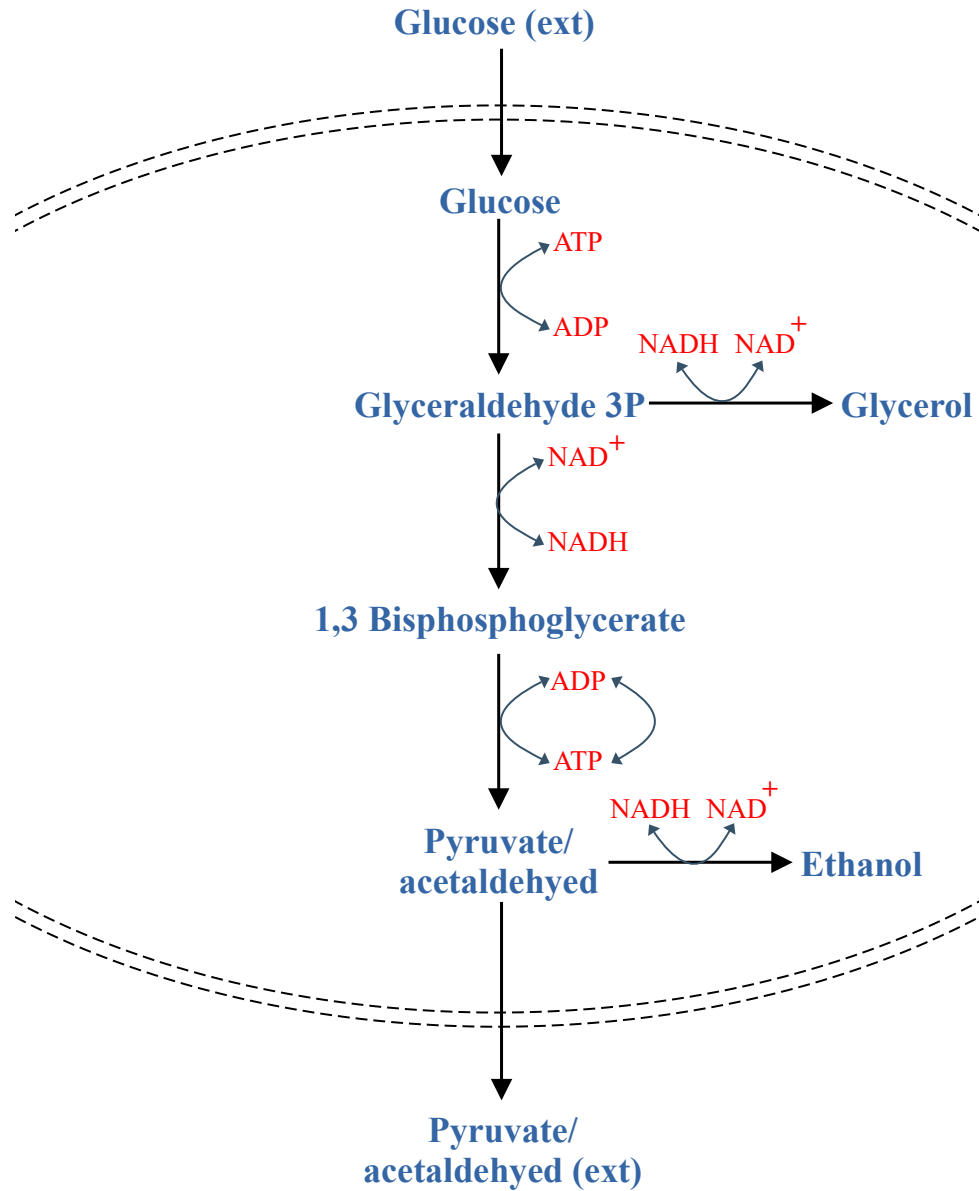


Figure S9. This figure depicts the main reactions of anaerobic glycolysis in a yeast cell¹⁰ together with the influx and outflux of glucose and pyruvateyacetaldehyde, respectively.

Table S22. Reaction list 3. It contains the list of 8 reactions of anaerobic glycolysis in a yeast cell¹⁰ under consideration.

-
1. Glucose external \Rightarrow Glucose
 2. Glucose + ATP \Rightarrow Glyceraldehyde 3P + ADP
 3. Glyceraldehyde 3P + NADH \Rightarrow Glycerol + NAD⁺
 4. Glyceraldehyde 3P + NAD⁺ \Rightarrow 1,3 Bisphosphoglycerate + NADH
 5. 1,3 Bisphosphoglycerate + ADP \Rightarrow Pyruvate/acetaldehyed + ATP
 6. ATP \Rightarrow ADP
 7. Pyruvate/acetaldehyed + NADH \Rightarrow Ethanol + NAD⁺
 8. Pyruvate/acetaldehyed \Rightarrow Pyruvate/acetaldehyed external
-

Table S23. Reaction ODE 3. It contains the list of 7 ordinary differential equations of anaerobic glycolysis in a yeast cell¹⁰ under consideration.

-
1. $\frac{d\text{glucose}}{dt} = J_0 - \frac{k_1.\text{glucose}.ATP}{1+(ATP/K_1)^q}$
 2. $\frac{dglyceraldehyde3P}{dt} = 2. \frac{k_1.\text{glucose}.ATP}{1+(ATP/K_1)^q} - k_2.\text{glyceraldehyde3P}.(N - NADH) - k_6.\text{glyceraldehyde3P}.NADH$
 3. $\frac{d1,3bisphosphoglycerate}{dt} = k_2.\text{glyceraldehyde3P}.(N - NADH) - k_3.1,3bisphosphoglycerate.(A - ATP)$
 4. $\frac{dpuryvate}{dt} = k_3.1,3bisphosphoglycerate.(A - ATP) - k_4.\text{pyruvate}.NADH - \kappa.(\text{pyruvate} - \text{pyruvate}(ext))$
 5. $\frac{dNADH}{dt} = k_2.\text{glyceraldehyde3P}.(N - NADH) - k_4.\text{pyruvate}.NADH - k_6.\text{glyceraldehyde3P}.NADH$
 6. $\frac{dATP}{dt} = -2. \frac{k_1.\text{glucose}.ATP}{1+(ATP/K_1)^q} + 2.k_3.1,3bisphosphoglycerate.(A - ATP) - k_5.ATP$
 7. $\frac{dpuryvate(ext)}{dt} = \phi.\kappa.(\text{pyruvate} - \text{pyruvate}(ext)) - k.\text{pyruvate}(ext)$
-

Table S24. IF–THEN rule base for FIS to capture fuzzy relationship between glucose & glucose & ATP & glyceraldehyde

IF (glucose & ATP)		Then glyceraldehyde 3P
glucose	ATP	glyceraldehyde
LOW	LOW	LOW
LOW	MEDIUM	LOW
LOW	HIGH	LOW
MEDIUM	LOW	LOW
MEDIUM	MEDIUM	MEDIUM
MEDIUM	HIGH	MEDIUM
HIGH	LOW	MEDIUM
HIGH	MEDIUM	MEDIUM
HIGH	HIGH	HIGH

Table S25. IF–THEN rule base for FIS to capture fuzzy relationship between glucose & 1,3 bisphosphoglycerate & ATP & pyruvate

IF (1,3 bisphosphoglycerate & ATP)		Then pyruvate
1,3 bisphosphoglycerate	ATP	pyruvate
LOW	LOW	LOW
LOW	MEDIUM	LOW
LOW	HIGH	LOW
MEDIUM	LOW	LOW
MEDIUM	MEDIUM	MEDIUM
MEDIUM	HIGH	MEDIUM
HIGH	LOW	MEDIUM
HIGH	MEDIUM	MEDIUM
HIGH	HIGH	HIGH

Table S26. We have employed the parameter values estimated by CRFIEKF, Ruoff et al.¹⁰ and Yazdani et al.⁹ to observe the dynamics of seven metabolites (as shown in the table) saperately. Afterwards, we have evaluated two set of MSEs that represents the difference between the dynamics in proposed technique and previous investigations^{9,10} individually. The significantly negligible MSEs of all the molecules indicates that the dynamics are indifferent in proposed method and previous researches^{9,10} Such a result clearly indicates the efficacy of the proposed technique.

Metabolite	MSE comparison	
	CRFIEKF vs Ruoff et al. ¹⁰	Yazdani et al. ⁹ vs Ruoff et al. ¹⁰
Glucose	0.0037	0.0001
Glyceraldehyde 3 phosphate	0.0012	0.0002
1,3-bisphosphoglycerate	0.0121	0.0001
pyruvate/acetaldehyde	0.0075	0.0001
NADH	0.0032	0.0001
ATP	0.0001	0.0004
pyruvate (external)	0.0057	0.0001

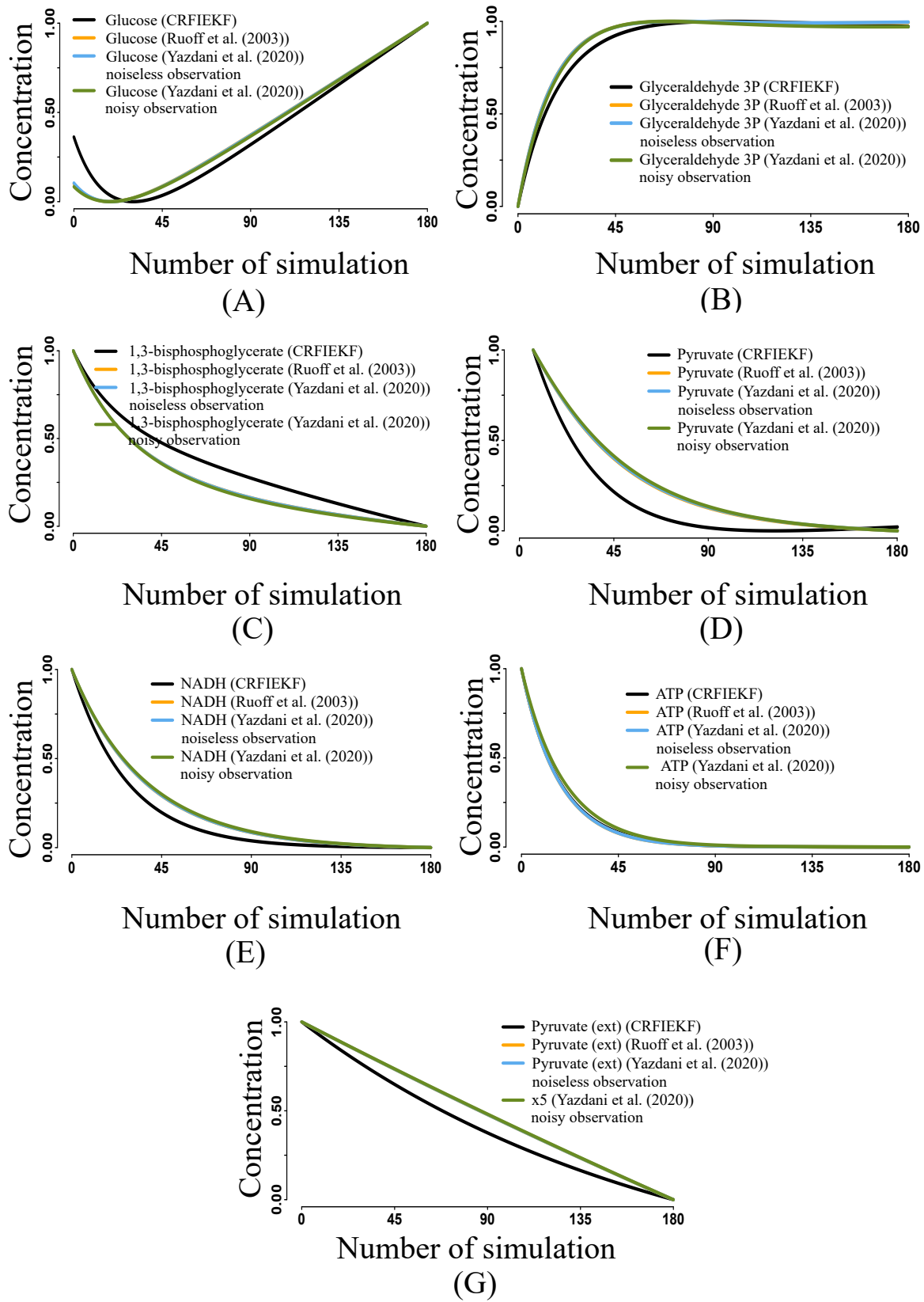


Figure S10. This figure depicts the dynamics seven metabolites using the parameter values estimated by proposed methodology and previous investigations^{9,10}. Here, $x_1, x_2, x_3, x_4, x_5, x_6$ and x_7 represents Glucose, Glyceraldehyde 3P, 1,3 Bisphosphoglycerate, Pyruvate, NADH, ATP and Pyruvate external respectively.

5. Parameter estimation of JAK-STAT signal transduction pathway

The JAK/STAT (Janus kinases/signal transducers and activators of transcription) pathway is a vital signal transduction pathway that plays a pivotal role in regulating the immune response^{11,12}. In this pathway, JAK represents a family of non-receptor tyrosine kinases, while STAT comprises functionally related proteins. The activation process begins with the binding of the ligand erythropoietin (Epo) to its receptor, leading to the phosphorylation of the receptor-associated JAK. This activation, in turn, triggers the phosphorylation of monomeric STAT. Subsequently, the monomeric STAT5 is transformed into its dimeric form, which enters the nucleus to initiate the transcription of target genes. Once its active role is complete, the dimerized Stat5 undergoes dedimerization and dephosphorylation. Consequently, the dephosphorylated Stat5 is transported back to the cytoplasm. You can refer to Supplementary Figure S11 for an illustration of the JAK/STAT signal transduction pathway. A detailed list of signaling interactions, along with the equations governing the interaction fluxes, can be found in Supplementary Table S27-S29.

To represent the known approximate relationships among the molecules, we categorized them into five linguistic values: ‘low’, ‘low-mid’, ‘medium’, ‘high-mid’, and ‘high’, considering a universe of discourse for the signal molecules within the range of [0,1]. The original parameter values, as estimated by the proposed method, along with the results from previous investigations^{13–15}, are presented in Supplementary Table S31. These results demonstrate the effectiveness of the proposed methodology.

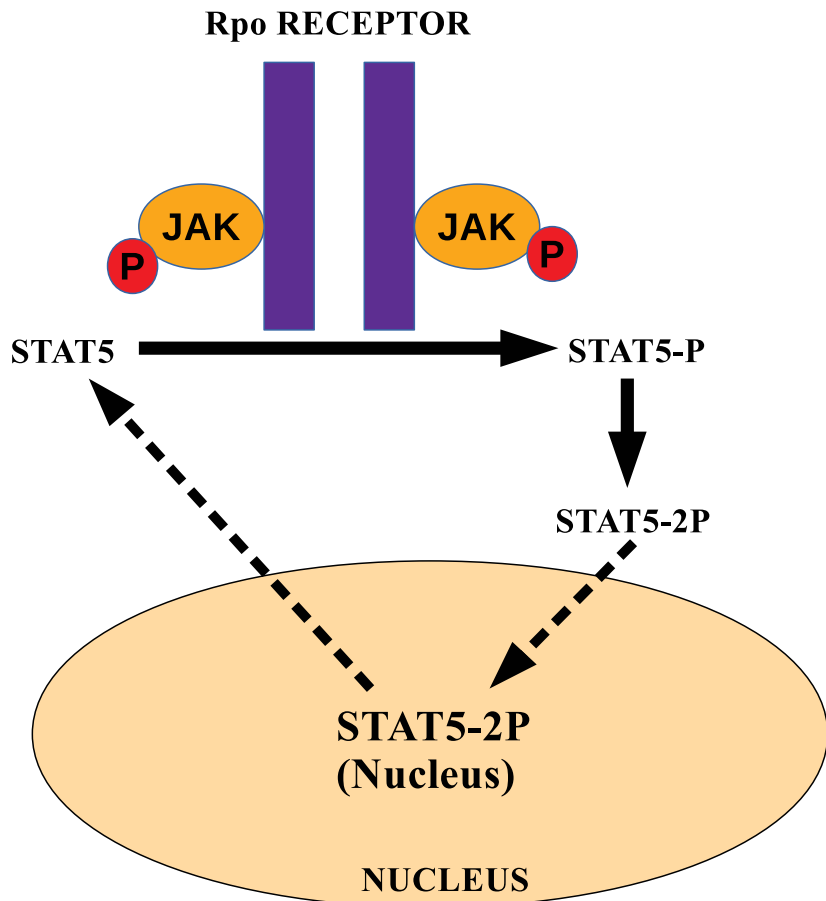


Figure S11. This figure depicts reduced JAK/STAT signal transduction pathway under consideration.

Table S27. Reaction list 4. It contains the list of 4 reactions from JAK/STAT signal transduction pathway under consideration. Here, the reaction numbers correspond to the same serial numbers in Table S16.

-
1. $EPO_R_A + STAT-5 \rightarrow STAT5-P$
 2. $2 STAT5-P \rightarrow STAT5-2P$
 3. $STAT5-2P \rightarrow STAT5-2P(NUCLEUS)$
 4. $STAT5-2P(NUCLEUS) \rightarrow 2 STAT-5$
-

Table S28. Reaction equations 4. It contains the list of equations of reaction fluxes associated with 4 reactions from JAK/STAT signal transduction pathway under consideration. Here the serial numbers correspond to the same reaction numbers in Table S15.

1. $v_1 = K_1 * [STAT5] * [EPOR_A]$
2. $v_2 = K_2 * [STAT5 - P] * [STAT5 - P]$
3. $v_3 = K_3 * [STAT5 - 2P]$
4. $v_4 = K_4 * [STAT5 - 2P(NUCLEUS)]$

Table S29. It contains the stoichiometric matrix associated with 4 reactions from JAK/STAT signal transduction pathway under consideration.

	v1	v2	v3	v4
STAT-5	-1	0	0	2
STAT5-P	1	-2	0	0
STAT5-2P	0	1	-1	0
STAT5-2P (NUCLEUS)	0	0	1	-1

Table S30. IF–THEN rule base for FIS to capture fuzzy relationship between Tyrosine phosphorylated STAT5 in cytoplasm & Total STAT5 in cytoplasm in JAK/STAT signal transduction pathway.

IF Tyrosine phosphorylated STAT5 THEN Total STAT5	
Tyrosine phosphorylated STAT5	THEN Total STAT5
VERY LOW	VERY LOW
LOW	SLIGHTLY HIGH
LOW	SLIGHTLY HIGH
LOW	LOW
MEDIUM	MEDIUM
SLIGHTLY HIGH	SLIGHTLY HIGH

Table S31. This table illustrates the parameter values of JAK/STAT signal transduction pathway using proposed method as well as previous investigations^{13–15}.

Kinetic Parameter	Parameter values comparison			
	Sun et. al (2008)	Swameye et al. (2003)	Sun et al. (2016)	CRFIEKF
k1	0.0211	0.021	0.022916	0.0201
k2	2.2788	2.46	2.343347	2.2003
k3	0.1064	0.1066	0.117178	0.1274
k4	0.1057	0.1066	0.102687	0.1305

6. IL6 dependent JAK-STAT3 Signal transduction pathway

IL6 plays a crucial role in regulating the inflammatory process. As depicted in Figure S12, the mechanism of initiating IL6 signal transduction, as shown in Heinrich et al.¹⁶, involves a series of steps. Initially, IL6 binds to its receptor subunit, glycoprotein 80 (IL6R), forming a complex. Two such complexes then bind to adaptor proteins of the glycoprotein 130 (gp130) type, resulting in the formation of a hexameric receptor complex denoted as (*R*_{complex}). Following the assembly of the receptor complex and the subsequent phosphorylation of gp130 ((*p*)*R*_{complex}), the signal transducer and transcription activator 3 (STAT3) protein are recruited into the phosphorylated gp130 complex. This, in turn, leads to the phosphorylation of STAT3 by the Jak protein, resulting in the formation of an active STAT3 dimer. The active STAT3 dimer goes on to influence several target genes, including Suppressors of Cytokine Signalling 3 (SOCS3) mRNAs and proteins, within the nucleus. For a more detailed understanding of the interactions among these proteins, please refer to the previous investigation by Haeseler et al.¹⁷.

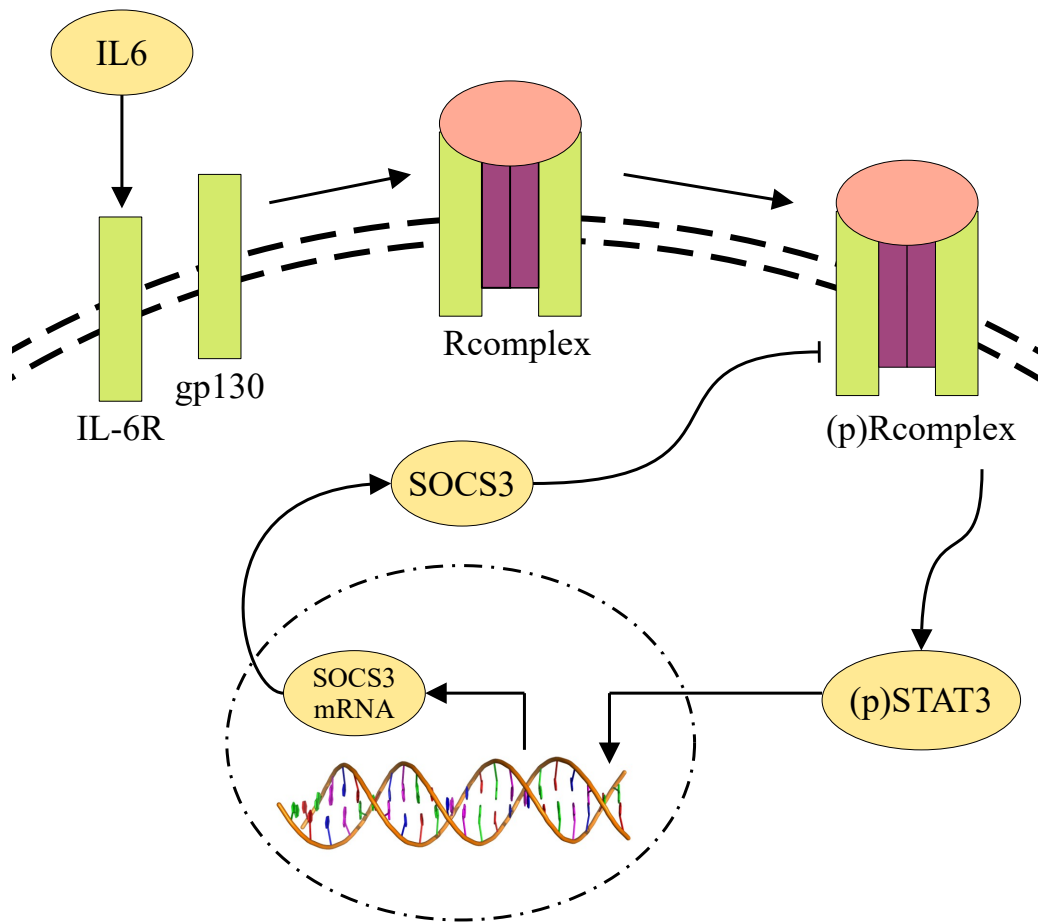


Figure S12. This figure depicts Schematic representation of IL6 dependent receptor complex assembly, Jak/STAT3 pathway activation and activation of target genes.

Table S32. Reaction ODE 5. It contains the list of 6 ordinary differential equations of IL-6-dependent Jak-STAT3 Signal transduction network¹⁷ under consideration.

1. $\frac{d(IL6 - IL6R)}{dt} = p_1 \cdot IL6R \cdot IL6 - p_2 \cdot (IL6 - IL6R) - 2 \cdot p_3 \cdot (gp130)^2 (IL6 - IL6R)^2 + 2 \cdot p_4 \cdot R_{complex}$
2. $\frac{dgp130}{dt} = 2 \cdot p_4 \cdot R_{complex} - 2 \cdot p_3 \cdot gp130^2 \cdot (IL6 - IL6R)^2$
3. $\frac{d(p)R_{complex}}{dt} = (p_5 \cdot R_{complex}) / (1 + p_{13} \cdot (SOCS3\ protein)) - p_6 \cdot (p)R_{complex}$
4. $\frac{d(p)STAT3}{dt} = p_7 \cdot (p)R_{complex} \cdot STAT3 - p_8 \cdot (p)STAT3$
5. $\frac{d(SOCS3\ mRNA)}{dt} = p_9 \cdot (p)STAT3 - p_{10} \cdot (SOCS3\ mRNA)$
6. $\frac{d(SOCS3\ protein)}{dt} = p_{11} \cdot (SOCS3\ mRNA) - p_{12} \cdot (SOCS3\ protein)$

Table S33. IF–THEN rule base for FIS to capture fuzzy relationship between gp130 & SOCS3 protein & (p)R_{complex}

IF (gp130 & SOCS3 protein)		Then (p)R _{complex}
gp130	SOCS3 protein	(p)R _{complex}
LOW	LOW	LOW
LOW	MEDIUM	LOW
LOW	HIGH	LOW
MEDIUM	LOW	MEDIUM
MEDIUM	MEDIUM	MEDIUM
MEDIUM	HIGH	LOW
HIGH	LOW	HIGH
HIGH	MEDIUM	MEDIUM
HIGH	HIGH	MEDIUM

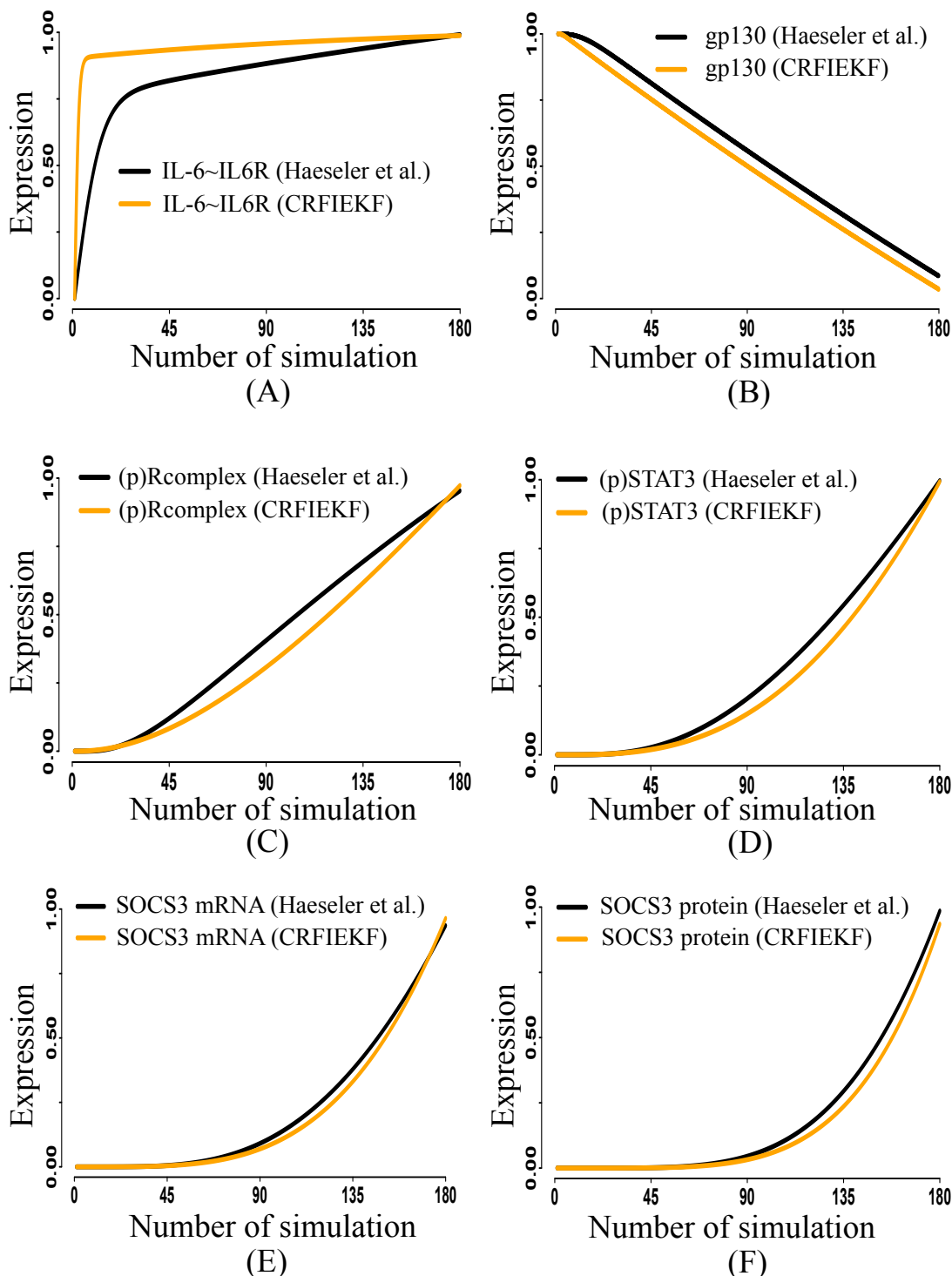


Figure S13. This figure depicts the dynamics (normalized in [0,1]) of six proteins of IL6 dependent JAK/STAT signal transduction pathway using parameter values estimated by the proposed technique and a previous investigation¹⁷.

Table S34. The table illustrates the parameter values estimated by proposed method as well as Haeseler et al.¹⁷

parameter	Proposed method	Haeseler et al.
p1	0.0100414	0.1218
p2	0.0100405	0.0388
p3	0.0100404	3.592
p4	0.0100385	0.0484
p5	0.0108882	0.0803
p6	0.0868793	0.0864
p7	0.0139551	0.156
p8	0.0100241	0.01
p9	0.010197	0.026
p10	0.0106126	0.021
p11	0.0195964	0.029
p12	0.0111405	0.008
p13	0.0854756	0.029

7. Parameter estimation of Ras/Raf/MEK/ERK signal transduction pathway

The Ras/Raf/MEK/ERK pathway is a vital mitogen-activated protein kinase (MAPK) signal transduction pathway that plays a pivotal role in controlling cell proliferation, differentiation, and survival^{18,19}. Furthermore, this cascade significantly influences apoptosis processes by phosphorylating various regulatory factors, including Bad, Bim, Mcl-1, and caspase-9²⁰. While the MAPK modules share structural components, they execute diverse biological functions. Growth factor receptors can activate proto-oncogenes like Ras and Raf-1 kinase, leading to ERK activation through phosphorylation and control of targeted gene transcription. In this study, we focused on a subset of the original pathway, as detailed by Sun et al.¹³ (illustrated in Figure S14). Specifically, we considered seven reactions from the Ras/Raf/MEK/ERK signal transduction pathway. The list of signaling interactions, along with equations describing interaction fluxes, is provided in Tables S35 to S37.

This truncated pathway involves 11 binding rate constants. Notably, we estimated the kinetic parameters without relying on experimental observations. To facilitate the estimation process, we developed a Fuzzy Inference System (FIS) to capture approximate relationships among four signaling molecules. As in previous cases, the linguistic variables in the FIS can take on three linguistic values: 'low,' 'medium,' and 'high.' Additionally, we assumed that the universe of discourse for metabolites and enzymes lies within the [0,1] range. The rule base for the FIS is detailed in Table S38. In the subsequent analysis, we presented the original parameter values and those estimated using our proposed technique, alongside results from previous investigations^{13,21,22}, in Table S39. Notably, we found that the sets of parameter values were statistically consistent at $p < 0.001$. Figure 5 in the original manuscript provides a visual comparison of the parameter values obtained through these different techniques.

Furthermore, we used the estimated parameter values to predict the dynamics of Raf-1* and RKIP. The predicted dynamics closely matched those observed in previous investigations¹³, as substantiated in Figure 6 of the original manuscript.

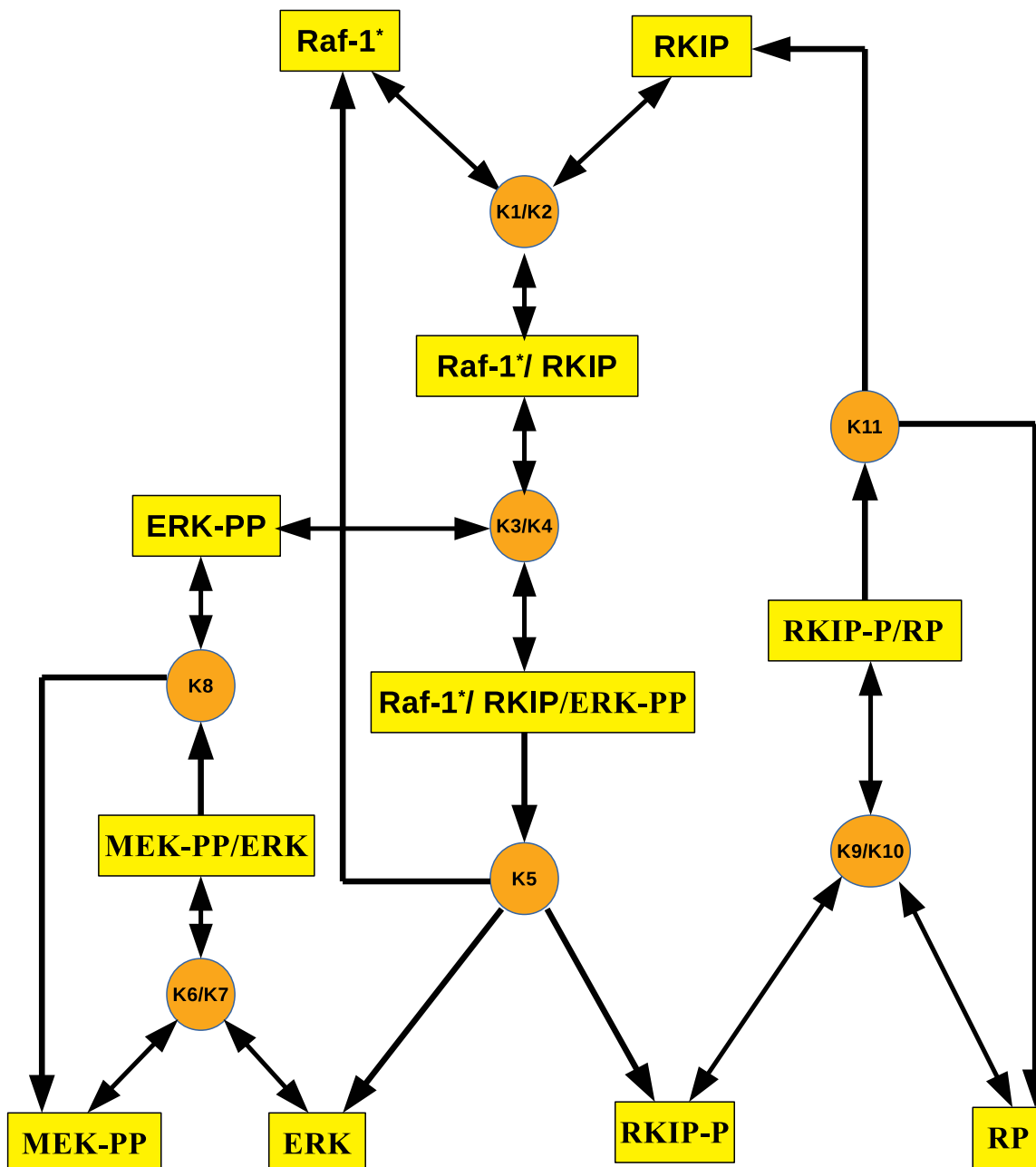


Figure S14. This figure depicts reduced Ras/Raf/MEK/ERK signal transduction pathway under consideration.

Table S35. Reaction list 6. It contains the list of 7 reactions from Ras/Raf/MEK/ERK signal transduction pathway under consideration. Here, the reaction numbers correspond to the same serial numbers in Table S21.

1. $\text{Raf-1}^* + \text{RKIP} \rightleftharpoons \text{Raf-1}^*/\text{RKIP}$
2. $\text{Raf1}^*/\text{RKIP} + \text{ERK-PP} \rightleftharpoons \text{Raf1}^*/\text{RKIP/ERK-PP}$
3. $\text{Raf1}^*/\text{RKIP/ERK-PP} \rightarrow \text{Raf-1}^* + \text{ERK} + \text{RKIP-P}$
4. $\text{MEK-PP} + \text{ERK} \rightleftharpoons \text{MEK-PP/ERK}$
5. $\text{MEK-PP/ERK} \rightarrow \text{MEK-PP} + \text{ERK-PP}$
6. $\text{RKIP-P} + \text{RP} \rightleftharpoons \text{RKIP-P/RP}$
7. $\text{RKIP-P/RP} \rightarrow \text{RKIP} + \text{RP}$

Table S36. Reaction equations 6. It contains the list of equations of reaction fluxes associated with 7 reactions from Ras/Raf/MEK/ERK signal transduction pathway under consideration. Here the serial numbers correspond to the same reaction numbers in Table S20.

1. $v_1 = K_1.[\text{Raf-1}^*].[RKIP-k2].[Raf-1^*/\text{RKIP}] - K_2.[\text{Raf-1}^*/\text{RKIP}]$
2. $v_2 = K_3.[\text{Raf-1}^*/\text{RKIP}].[ERK-PP-k4].[Raf-1^*/\text{RKIP/ERK-PP}] - K_4.[\text{Raf-1}^*/\text{RKIP/ERK-PP}]$
3. $v_3 = K_5.[\text{Raf-1}^*/\text{RKIP/ERK-PP}]$
4. $v_4 = K_6.[\text{ERK}].[MEK-PP-k7].[MEK-PP/\text{ERK}] - K_7.[\text{MEK-PP}/\text{ERK}]$
5. $v_5 = K_8.[\text{MEK-PP}/\text{ERK}]$
6. $v_6 = K_9.[\text{RKIP-P}].[RP]-k10.[\text{RKIP-P}/\text{RP}]$
7. $v_7 = K_{11}.[\text{RKIP-P}/\text{RP}]$

Table S37. It contains the stoichiometric matrix associated with 7 reactions from Ras/Raf/MEK/ERK signal transduction pathway under consideration.

	v1	v2	v3	v4	v5	v6	v7
Raf-1*	-1	0	1	0	0	0	0
RKIP	-1	0	0	0	0	0	1
Raf-1^*/RKIP	1	-1	0	0	0	0	0
Raf-1^*/RKIP/ERK-PP	0	1	-1	0	0	0	0
ERK	0	0	1	-1	0	0	0
RKIP-P	0	0	1	0	0	-1	0
MEK-PP	0	0	0	-1	1	0	0
MEK-PP/ERK	0	0	0	1	-1	0	0
ERK-PP	0	-1	0	0	1	0	0
RP	0	0	0	0	0	-1	1
RKIP-P/RP	0	0	0	0	1	-1	0

Table S38. IF–THEN rule base for FIS to capture fuzzy relationship between MEK-PP & RP and MEK-PP/ERK & ERK-PP in Ras/Raf/MEK/ERK signal transduction pathway.

IF (MEK-PP & RP)		THEN (MEK-PP/ERK & ERK-PP)	
MEK-PP	RP	MEK-PP/ERK	ERK-PP
LOW	LOW	LOW	HIGH
LOW	MEDIUM	MEDIUM	MEDIUM
LOW	HIGH	MEDIUM	LOW
MEDIUM	LOW	HIGH	LOW
MEDIUM	MEDIUM	MEDIUM	MEDIUM
MEDIUM	HIGH	MEDIUM	LOW
HIGH	LOW	LOW	MEDIUM
HIGH	MEDIUM	HIGH	LOW
HIGH	HIGH	HIGH	LOW

Table S39. This table illustrates the parameter values of Ras/Raf/MEK/ERK signal transduction pathway using proposed method as well as previous investigations^{13,21,22}

Kinetic Parameter	Parameter values comparison			
	Sun et. al (2008)	Kwang et al. (2003)	Capinski et al.(2016) (Classical)	CRFIEKF
k1	0.5242	0.53	0.05227	0.501
k2	0.0075	0.0072	0.0078	0.0077
k3	0.6108	0.625	0.6615	0.5907
k4	0.0025	0.00245	0.002	0.0537
k5	0.0371	0.0315	0.0312	0.0081
k6	0.8101	0.8	0.7922	0.8305
k7	0.0713	0.0075	0.0073	0.0955
k8	0.0687	0.071	0.0711	0.0594
k9	0.96	0.92	0.9207	0.9241
k10	0.0012	0.00122	0.0014	0.0033
k11	0.872	0.87	0.8622	0.7589

References

1. Jia G, Stephanopoulos G, Gunawan R. Incremental parameter estimation of kinetic metabolic network models. *BMC systems biology* 2012;6(1):142.
2. Voit EO, Almeida J. Decoupling dynamical systems for pathway identification from metabolic profiles. *Bioinformatics* 2004;20(11):1670–1681.
3. Nelson DL, Lehninger AL, Cox MM. Lehninger Principles of Biochemistry. Macmillan; 2008.
4. Bolaños JP, Almeida A, Moncada S. Glycolysis: a bioenergetic or a survival pathway? *Trends in biochemical sciences* 2010;35(3):145–149.
5. Paul D, Dasgupta A, De RK. Exploring the altered dynamics of mammalian central carbon metabolic pathway in cancer cells: a classical control theoretic approach. *PloS one* 2015;10(9):e0137728.
6. Kanehisa M, Goto S. Kegg: kyoto encyclopedia of genes and genomes. *Nucleic acids research* 2000;28(1):27–30.
7. Lillacci G, Khammash M. Parameter estimation and model selection in computational biology. *PLoS computational biology* 2010;6(3):e1000696.
8. Kinoshita A, Tsukada K, Soga T, Hishiki T, Ueno Y, Nakayama Y, Tomita M, Suematsu M. Roles of hemoglobin allostericity in hypoxia-induced metabolic alterations in erythrocytes: simulation and its verification by metabolome analysis. *Journal of Biological Chemistry* 2007;
9. Yazdani A, Lu L, Raissi M, Karniadakis GE. Systems biology informed deep learning for inferring parameters and hidden dynamics. *PLoS computational biology* 2020;16(11):e1007575.
10. Ruoff P, Christensen MK, Wolf J, Heinrich R. Temperature dependency and temperature compensation in a model of yeast glycolytic oscillations. *Biophysical chemistry* 2003;106(2):179–192.
11. Mertens C, Darnell JE. Snapshot: Jak-stat signaling. *Cell* 2007;131(3):612.
12. Villarino AV, Kanno Y, O’Shea JJ. Mechanisms and consequences of jak–stat signaling in the immune system. *Nature immunology* 2017;18(4):374.
13. Sun X, Jin L, Xiong M. Extended kalman filter for estimation of parameters in nonlinear state-space models of biochemical networks. *PloS one* 2008;3(11):e3758.
14. Swameye I, Müller T, Timmer J, Sandra O, Klingmüller U. Identification of nucleocytoplasmic cycling as a remote sensor in cellular signaling by databased modeling. *Proceedings of the National Academy of Sciences* 2003;100(3):1028–1033.
15. Sun X, Medvedovic M. Model reduction and parameter estimation of non-linear dynamical biochemical reaction networks. *IET systems biology* 2016;10(1):10–16.
16. Heinrich P. Behrmann i, haan s, hermanns hm, muller-newen g, and schaper f. *Principles of interleukin (IL)-6-type cytokine signalling and its regulation* *Biochem J* 2003;374:1–20.
17. Haeseler Fv, Rudolph N, Findeisen R, Huber HJ. Parameter estimation for signal transduction networks from experimental time series using picard iteration. *IFAC-PapersOnLine* 2018;51(18):191–196.
18. Kolch W. Meaningful relationships: the regulation of the ras/raf/mek/erk pathway by protein interactions. *Biochemical Journal* 2000;351(2):289–305.
19. Chowdhury I, Thompson WE, Thomas K. Prohibitins role in cellular survival through ras-raf-mek-erk pathway. *Journal of cellular physiology* 2014;229(8):998–1004.
20. Li L, Zhao GD, Shi Z, Qi LL, Zhou LY, Fu ZX. The ras/raf/mek/erk signaling pathway and its role in the occurrence and development of hcc. *Oncology letters* 2016;12(5):3045–3050.
21. Kwang-Hyun C, Sung-Young S, Hyun-Woo K, Wolkenhauer O, McFerran B, Kolch W. Mathematical modeling of the influence of rkip on the erk signaling pathway. In: *International Conference on Computational Methods in Systems Biology*. Springer; 2003:127–141.
22. Capinski M, Polanski A. Parameter estimation in systems biology models by using extended kalman filter. In: *Man–Machine Interactions 4*. Springer; 2016:195–204.